DANMARKS OG GRØNLANDS GEOLOGISKE UNDERSØGELSE RAPPORT 2008/37

Evaluation of the future hydropower potential at Paakitsoq, Ilulissat, West Greenland

Technical Report

Andreas Peter Ahlstrøm, Ruth Mottram, Claus Nielsen,
Niels Reeh & Signe Bech Andersen

GEOLOGICAL SURVEY OF DENMARK AND GREENLAND
MINISTRY OF CLIMATE AND ENERGY

GEUS

DANMARKS OG GRØNLANDS GEOLOGISKE UNDERSØGELSE RAPPORT 2008/37

Evaluation of the future hydropower potential at Paakitsoq, Ilulissat, West Greenland

Technical Report

Andreas Peter Ahlstrøm, Ruth Mottram, Claus Nielsen,
Niels Reeh & Signe Bech Andersen

GEOLOGICAL SURVEY OF DENMARK AND GREENLAND
MINISTRY OF CLIMATE AND ENERGY

GEUS

Contents

Summary

This technical report presents an evaluation of the future runoff conditions from the hydrological basin Paakitsup Akuliarusersua near Ilulissat, West Greenland. It supplements a similar titled summary report (published as GEUS Report 31/2008) by providing a more complete background, more of the intermediate results and appendices with flow charts describing step-by-step how these results were obtained. The glaciological evaluation presented here also forms a continuation of previous glaciological activities by the Geological Survey of Denmark and Greenland related to hydropower in the Paakitsoq region, as summarized in a previous report by Ahlstrøm (2007).

The Paakitsup Akuliarusersua basin, often termed Paakitsoq after the nearby bay, is complicated because it is mainly supplied by meltwater from the ice-sheet margin, requiring glaciological modelling of future ice-sheet behaviour. The evaluation presented here is based on all the available observational data for the region, the most recent climate model scenario and state-of-the art ice-sheet models for ice dynamics and meltwater hydrology. The main results can be summarized as follows:

- The configuration of the ice-sheet hydrological basin is likely to remain constant until at least 2080.
- As a minimum, the basin discharge is likely to remain constant until 2035, followed by a steady increase towards 2080.
- The ice-sheet margin is likely to keep thinning at the current rate of approximately 1 metre per year.

The lakes adjoining the ice-sheet margin in the Paakitsoq basin are sensitive to changes in drainage pathways and general configuration. Outlet changes have already occurred twice within the last two decades, as a consequence of the steady retreat of the ice-margin. Even with a stable ice-margin, lakes adjoining the ice margin can undergo cycles with slow filling interrupted by sudden catastrophic outburst floods, as the water pressure becomes large enough to lift the ice damming the lake. A small readvance of the ice margin in the Paakitsoq region may re-establish previous lake outlets, separating once more the northern and southern parts of the basin. Although a steady future retreat of the ice margin is predicted, modelling of ice-sheet margins on a sub-kilometre scale is not accurate. Changes in the parameters controlling basal sliding, such as meltwater supply to the subglacial drainage, may cause a minor advance. Thus, it is advised to take precautions against a minor readvance of the ice margin even if such an event is not predicted.

1. Introduction

The ice-sheet margin terminating in the Paakitsoq region of West Greenland has seen a wide variety of scientific activities for more than half a century. These activities have accelerated due to the interest in developing the region for hydropower providing ample opportunities for science, either as part of the ongoing glaciological investigations or through the support offered by the existing logistics. The ice sheet margin at Paakitsoq is now a scientifically well known locality, since the ice appears at the surface only slightly disturbed chronologically, implying that it is possible to some extent to mine ice from a specific period. This has opened possibilities for retrieving very large samples necessary for some types of palaeoclimatological analyses, such as investigating the origin of the sudden atmospheric methane increase occurring at the transition between the last ice-age and the present warm period by ^{14}C-dating the carbon in the methane trapped in air bubbles in the ice sheet. The Paakitsoq locality is also known among scientists because of the Swiss Camp, a science facility started by ETH Zürich and later taken over by University of Colorado. It was at this site that firm evidence of a connection between surface meltwater production and ice sheet velocity was first obtained (Zwally and others, 2002). Past work on the hydropower potential of the area has been summarised by Ahlstrøm (2007) broadly covering the period from the early 1980s to the early 1990s. In the following work, the annual discharge has been estimated for the whole catchment extending to the year 2080, with the contribution from the largest sub-basin specified on its own. The final result is shown in Figure 41. Predicting future run-off conditions from a hydrological basin containing an ice sheet is a difficult and uncertain task due to the inherent complexity of the system. Nevertheless, it is possible to constrain and account for the range of likely variability within the system. This report aims to describe the procedure by which future predictions have been made and to indicate the uncertainties and sources of error within the techniques used. There were several distinct stages in the study and the layout of this report broadly follows them:

- Measuring and constructing maps of surface and basal topography
- Climate modelling and downscaling output to local topography
- Predicting mass balance based on climate model output
- Modelling melt rates
- Ice-dynamics modelling
- Basin analysis and discharge calculations

The discharge estimate relies on a particular choice for the future global greenhouse gas emissions, namely the IPCC SRES B2 scenario[a]. This particular emission scenario was originally chosen by the Danish Meteorological Institute for their combined global/regional climate model run because it represented the “middle of the road” in the family of scenarios. The B2 scenario is now believed to be fairly conservative in its predictions. That implies that the discharge estimate provided here is most likely also conservative, as most of the

[a] IPCC SRES: Intergovernmental Panel for Climate Change - Special Report on Emission Scenarios

water comes from ice sheet melt, a process which is particularly sensitive to predicted rise in air temperature and changes in precipitation. The conclusion is that with a fairly conservative climate evolution scenario, the discharge is predicted to remain relatively constant on average until 2035, at which point a steady increase in the discharge sets in. This prediction includes the response of the ice-sheet margin to climate change in terms of ice dynamic changes and mass balance and is robust for the range of realistic basal water pressures, that might otherwise cause changes in the delineation of the ice-sheets hydrological basins.

A range of observational data was required for the glaciological modelling, including hydrological and climatological data series collected by the Greenland Survey (Asiaq), used for the purposes of calibrating model output. Airborne elevation and ice-thickness measurements derived from radar and lidar measurements collected and processed by the National Space Institute at the Technical University of Denmark were used to define the surface topography and thickness of the ice sheet. A detailed surface topography for the ice-free part of the basin, based on stereophotogrammetry, was supplied by the Department of Geological Mapping of the Geological Survey of Denmark and Greenland (GEUS). The ice dynamic and melt models were driven by output from a combined global/regional climate model (HIRHAM4) forced by the IPCC SRES B2 scenario and run by the Danish Meteorological Institute (DMI). Other data, including existing ice sheet observations from GEUS and from US automatic weather stations (GC-Net), were used to verify and calibrate modelling work.

2. Surface topography and ice thickness

2.1 Radar and Lidar Processing and Interpretation

To characterise the current ice-sheet margin we used a combination of existing and new data including ice-penetrating radar to determine subglacial topography and laser altimeter measurements to determine the current surface elevation. The new data were collected in 2005 during 5 hours of flying with flight tracks roughly 1 km apart in the Paakitsoq marginal area (shown in Figure 1). The data collection was funded by the Commission for Scientific Research in Greenland in anticipation of the likely interest in future hydropower development. Measurements were made with a 60 MHz coherent radar system and a scanning laser altimeter (lidar). Positioning was accomplished with several onboard differential Global Positioning Systems (dGPS) and aircraft orientation with an inertial navigation system (INS).

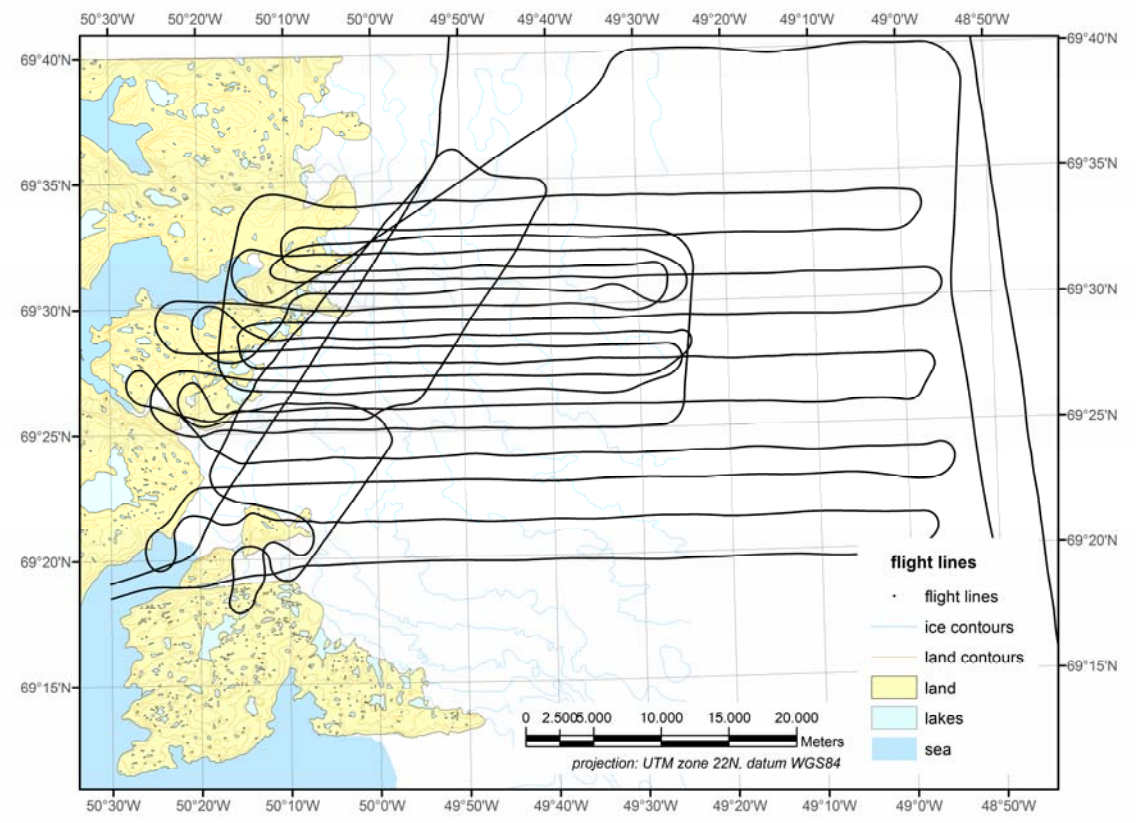

Figure 1. *Flight lines from the ice sheet survey in 2005. The survey was designed to facilitate a future investigation of the hydropower feasibility at Paakitsoq and is thus more dense in the most critical part of the ice sheet margin, with a track spacing down to approx. 1 km.*

Radar and lidar work in a similar fashion, by emitting electromagnetic radiation and measuring how quickly it returns to the transmitter/receiver, the location of which is fixed using a connected GPS system. Lidar does not penetrate the ice surface but radar by contrast, can reveal two reflections, one from the ice surface and a second one from the subglacial bed. Liquid water in crevasses and voids reflects and attenuates the signal, often making it difficult to use radar when water is abundant. The output of the technique is a radargram (see Figure 2A) that is further processed to give topographic elevations.

The radar data collected in 2005 were processed by the National Space Institute at DTU, following a new processing chain to optimise the radargrams and reformatted to conform to the standard RAMAC format. Reflection and attenuation within the ice-sheet reduces the strength of the returned echo. Substantial processing is therefore required to produce a radargram that makes detection of the ice-sheet bottom echo possible and is done both on-line during acquisition and off-line using software developed at the Microwave & Remote Sensing section, DTU-Space. This processing consists of coherent filtering to suppress unwanted signal components and noise, followed by incoherent averaging to reduce speckle noise. Examples of the raw and processed radargrams are given in Figures 2A and 2B respectively.

Reflections were visually identified and digitized using the ReflexW© software and the bed and surface elevation were calculated from the digitized lines. The interpretation required the visual identification and digitizing of surface and bed radar reflection for some 85,000

different points. There was little or no evidence of continuous internal layers which might have been useful for understanding the dynamics of the ice margin.

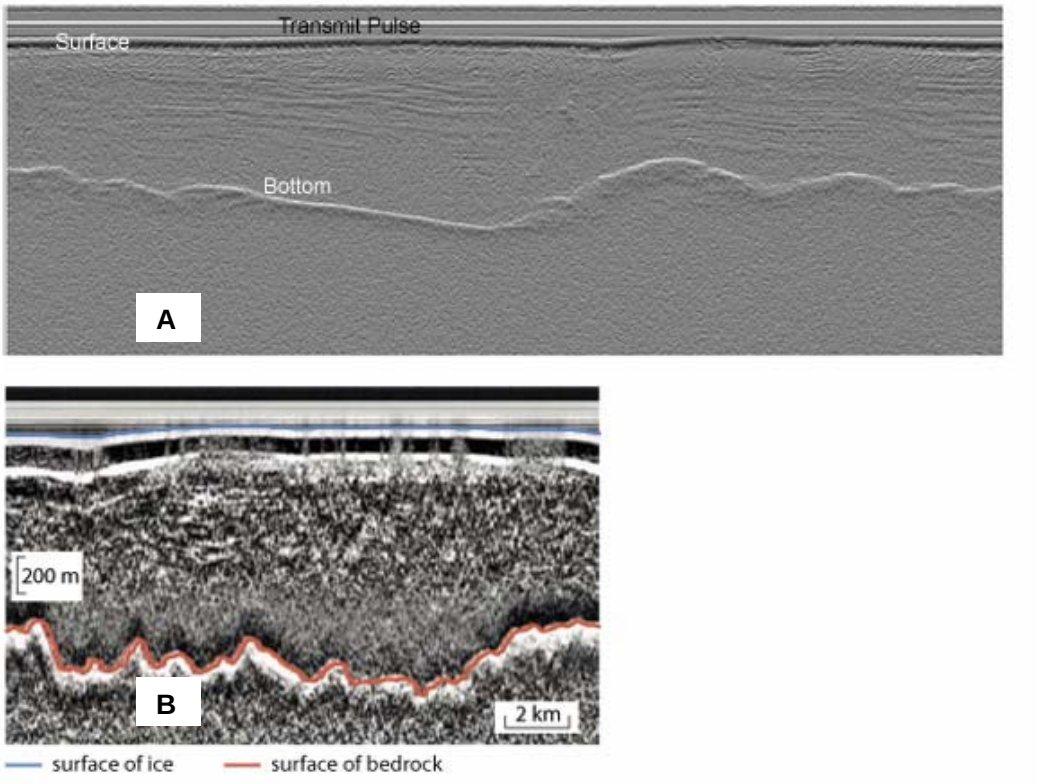

Figure 2. *Radargrams illustrating bed and surface topographic traces taken from two different places within the region. A shows the initial radargram, obtained from the sounder. B displays the processed radargram with the digitised traces of the surface layer shown in blue and the bottom returns shown in red.*

The two way travel time of the radar pulse from the plane to the basal and surface layers and the elevation of the plane above the WGS84 ellipsoid, determined by dGPS position, were used to calculate the surface elevation (equation 1) from which the ice thickness could be derived (equation 2).

$$H_s = H_p - 0.5 \cdot t_S v_{air} \quad (1)$$

The surface elevation, H_S, is determined using the measured elevation of the plane, H_p, the two-way travel time to the surface, t_s, and the velocity of light through air, v_{air}. The factor 0.5 is applied to give the one-way travel time.

$$H_i = 0.5 \cdot (t_B - t_S) \cdot v_{ice} \quad (2)$$

The ice thickness, H_i is derived from t_b, the two way travel time to the bed and v_{ice}, the velocity of light through ice. The bed elevation, H_b, is then simply calculated by subtracting the ice thickness from the surface elevation (equation 3).

$$H_b = H_s - H_i \quad (3)$$

All elevations are given relative to the standard WGS84 ellipsoid as the local correction to sea level is not well known. The speed of the radar pulse through air was assumed to be 0.3 m/ns and through ice 0.169 m/ns (Bogorodsky and others, 1985; Hempel and others, 2000).

Surface elevation data was derived from laser altimeter measurements made concurrently with the radar measurements and using the same INS and GPS set up to derive positioning information. A Riegl scanning laser was used to make the elevation measurements, which provides cross-track scans with a range accuracy better than 5 cm. Absolute elevations are given with a precision of ±0.3 m following processing. The laser operates in the near-infrared wavelength band and has a scan angle of 60°, giving a swath width similar to the flight elevation above the ground. Post-processing to combine positional and elevation information in vector format files was carried out at the Geodynamics Department of DTU-Space.

Since the surface reflections were not visible over large parts of the radargrams, and the precision of the lidar is an order of magnitude higher in quality than the radar, the lidar data were superior to the radar for calculating the surface elevation. The radar elevations are known with a precision of ± 80 m and lidar elevations are given a precision of ± 0.3 m. Using the geographical positioning information the two datasets could be matched up precisely and combined. With the assistance of local maps, the data could be divided into bare rock elevation (outside of the ice sheet), bedrock elevation (below the ice sheet) and ice-sheet surface elevation. These data sets were then used for the construction of the digital terrain models (DTM).

2.2 Digital Terrain Modelling

Previous work (Ahlstrøm and others, 2007) with similar data sets has shown that the geostatistical interpolation method known as block kriging is superior for creating regular grids from the airborne radar and lidar data. Kriging is used to estimate elevation at an unobserved location from observations at nearby locations. In making each calculation, the algorithm applies more weight to the values of locations closer to the unknown point and less weight to observations from farther away. It is a particularly powerful technique for topographic interpolation, as the algorithms can also be used to take into account the directional variability of topography. That is, in some directions topography may have greater variability than in other directions around a known point, this is particularly true in areas of high relief. Although the principle is simple, there are some extra complexities, particularly when using data for which there is substantial uncertainty, as with the absolute basal elevations. This is the so-called ‘nugget effect’ which takes into account both the repeatability of each individual measurement, the error variance, and the uncertainty in each measured location, the micro variance, in this case ±80 m.

The core of using the kriging technique is the semivariogram, usually abbreviated to the variogram. This is a measure of how quickly a quantity, in this case elevation, changes on the average. The variogram is also a function of direction, since it represents three variables; two independent variables, the direction and the separation distance; and one dependent variable known as the variogram value, a function of the two independent vari-

ables. The plotted variogram is a radial slice (like a piece of pie) from a grid of these 3 variables and it is therefore necessary to examine multiple variograms when fitting a model as it is difficult to both draw a three-dimensional surface and to fit a three dimensional function to it. By taking slices, an XY plot can be used to work with the directional experimental variogram. Ultimately the variogram model must be applicable to all directions fitting the model. Examples of variogram plots are shown in Figure 3, in these the lag distance (the separation distance between pairs of points) is plotted on the x-axis, and the variogram function is shown on the y-axis. The plot therefore shows how elevations vary with distance from a given point.

A block kriging algorithm (Kitanidis, 1997), based on a rational quadratic model and incorporating an adjustment for the nugget effect, was developed using plotted semivariograms in 8 directions to take into account a priori knowledge of bed topographic variability (Ahlstrøm and others, 2002, 2005). Figure 3 shows the modelled and measured semivariograms for 4 different angles and, as the figure shows, although the selected model works better in some directions than others, it was found to be the best compromise for variability in the full directional range.

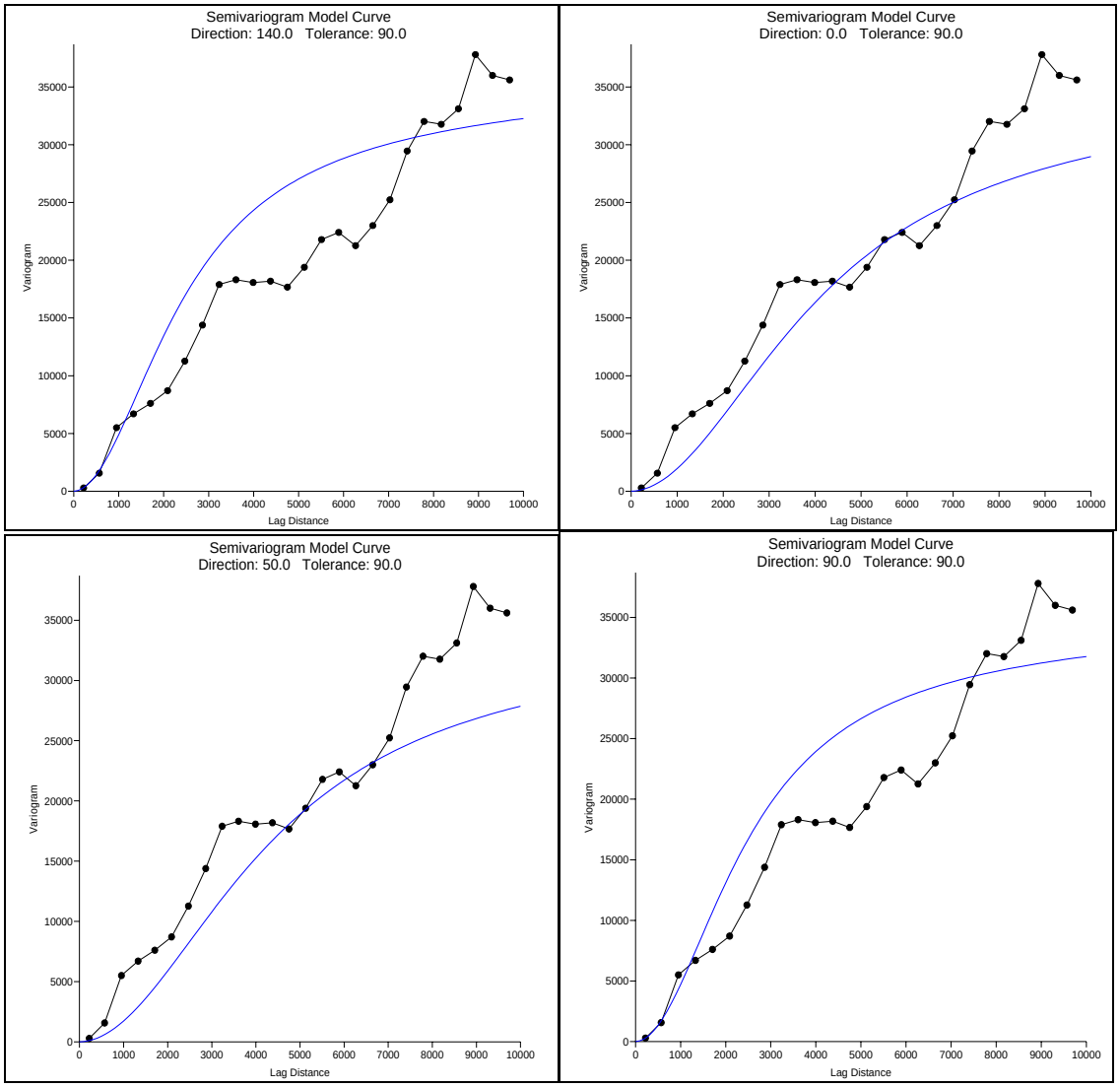

Figure 3. *Four variograms illustrating the fit of the model curve (blue line) to the plotted data points ín four different directions for the bedrock topography.*

For the ice surface topographic data set a linear model was found to work best, probably since the ice flow acts to linearise and smooth out topographic variability, as shown in the variogram in Figure 4.

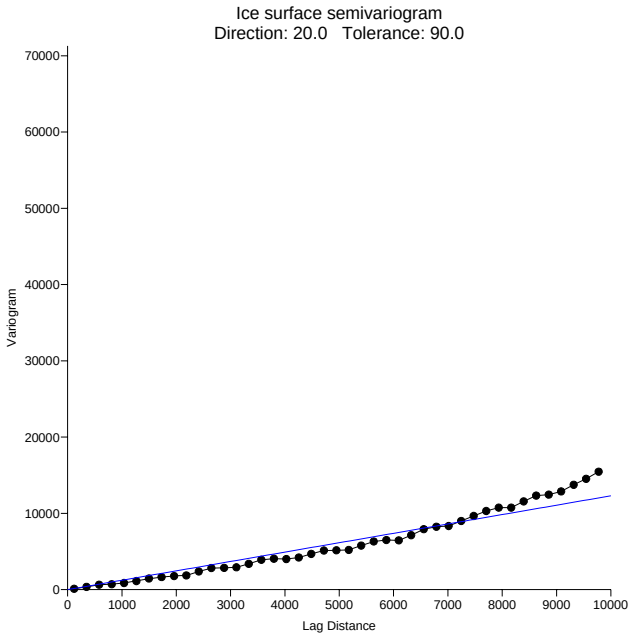

Figure 4. *Linear variogram model for the ice surface topography.*

The variograms were used to apply a kriging algorithm to the radar and lidar datasets in order to interpolate elevations in areas with poor coverage of data points. The initial DEMs created using the kriged radar and lidar data are shown in Figures 5 and 6. They cover the Paakitsoq area well, but to study both the hydrology and ice dynamics information over a much broader area was necessary and therefore the local DEMs were merged with other datasets.

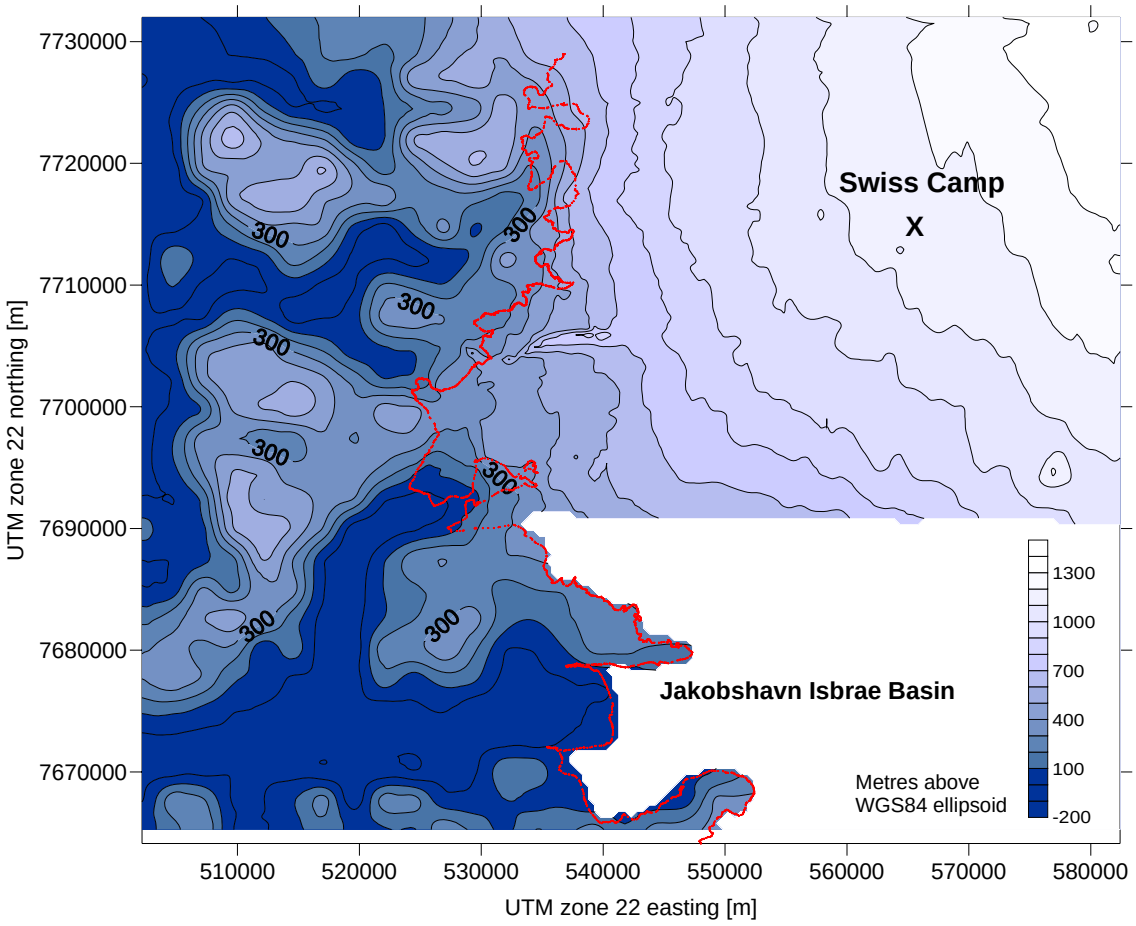

Figure 5. *The new surface topography map showing both ice free and currently ice covered terrain. The red line indicates the ice sheet margin. Both this and the topography outside the ice sheet are taken from the GEUS DEM of the area created from aerial photos taken in 1985. The white space represents the area not covered in this study. The map is in UTM22 coordinates (Northing [m] and Easting [m]), datum WGS-84*

Figures 5 and 6 present maps of the ice surface and the basal topography for the Pakitsoq region, based predominantly on the flight lines shown in Figure 1 as well as the GEUS dataset described below. The red line indicates the ice margin mapped from aerial photographs taken in 1985 (Thomsen and others, 1986). The Jakobshavn outlet glacier, which has since retreated from the position shown was not covered by this study. The position of the Swiss Camp research base is also shown on both maps.

Surface topographic contours show the large scale trend of sloping down towards the margin, and also south towards the Jakobshavn basin. The resolution of the grid does not allow small-scale features such as melt ponds and run-off channels to be discerned.

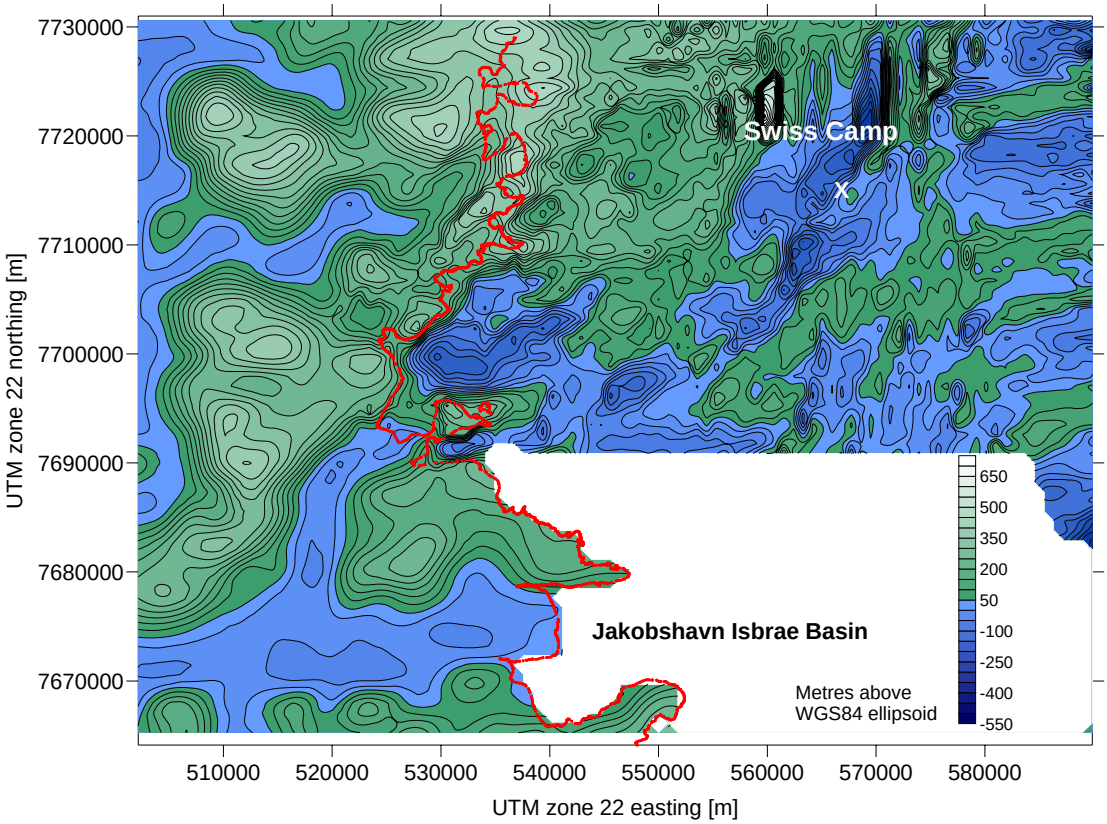

Figure 6. *Basal topographic map showing both ice free and currently ice covered terrain. The red line indicates the ice sheet margin. Both this and the topography outside the ice sheet are taken from the GEUS DEM of the area created from aerial photos taken in 1985. The white space represents the area not covered in this study. The map is in UTM22 coordinates (Northing [m] and Easting [m]), datum WGS-84.*

The basal topographic map in Figure 6 shows that the hilly ice-free terrain continues part way underneath the current ice cover, with a large feature, reaching elevations of around 500 m in the north of the area. Further inland however, the topography becomes much more low-lying with large parts of the area at or below the ellipsoidal datum, and therefore likely to be below sea level. A large valley system with a significant over deepening is shown behind the current calving front of the outlet glacier extending several kilometres back. A large trough is also identifiable at Swiss Camp, significantly, both these features also show on the subglacial topography given by Thomsen and others (1986), giving additional confidence in the results. As with the outlet glacier trough, the Swiss camp feature also trends broadly northeast to southwest. The small irregular features to the north are likely to be artefacts of the kriging and gridding process, as data coverage in this area was rather poor, possibly due to the large volume of meltwater expected in this area close to the ablation zone. Nevertheless, comparison with the earlier survey data (Thomsen and others, 1986) also shows similar features in the same location, so it is likely that at least part of the topographical undulations are real.

To set the lidar and radar derived DEMs in their local context, they were merged with GEUS data from an airborne stereophotogrammetric survey carried out in 1985. This data was initially used to produce high-resolution vector maps of the topography and prominent

landscape features with special focus on topography in ice free areas (Thomsen and others, 1988). The vector map data was reprocessed for physical modelling purposes including extraction of the relevant points, polylines and polygons from the vector data, and it was transformed into a standard DEM, suitable as input for numerical models (see Figure 7).

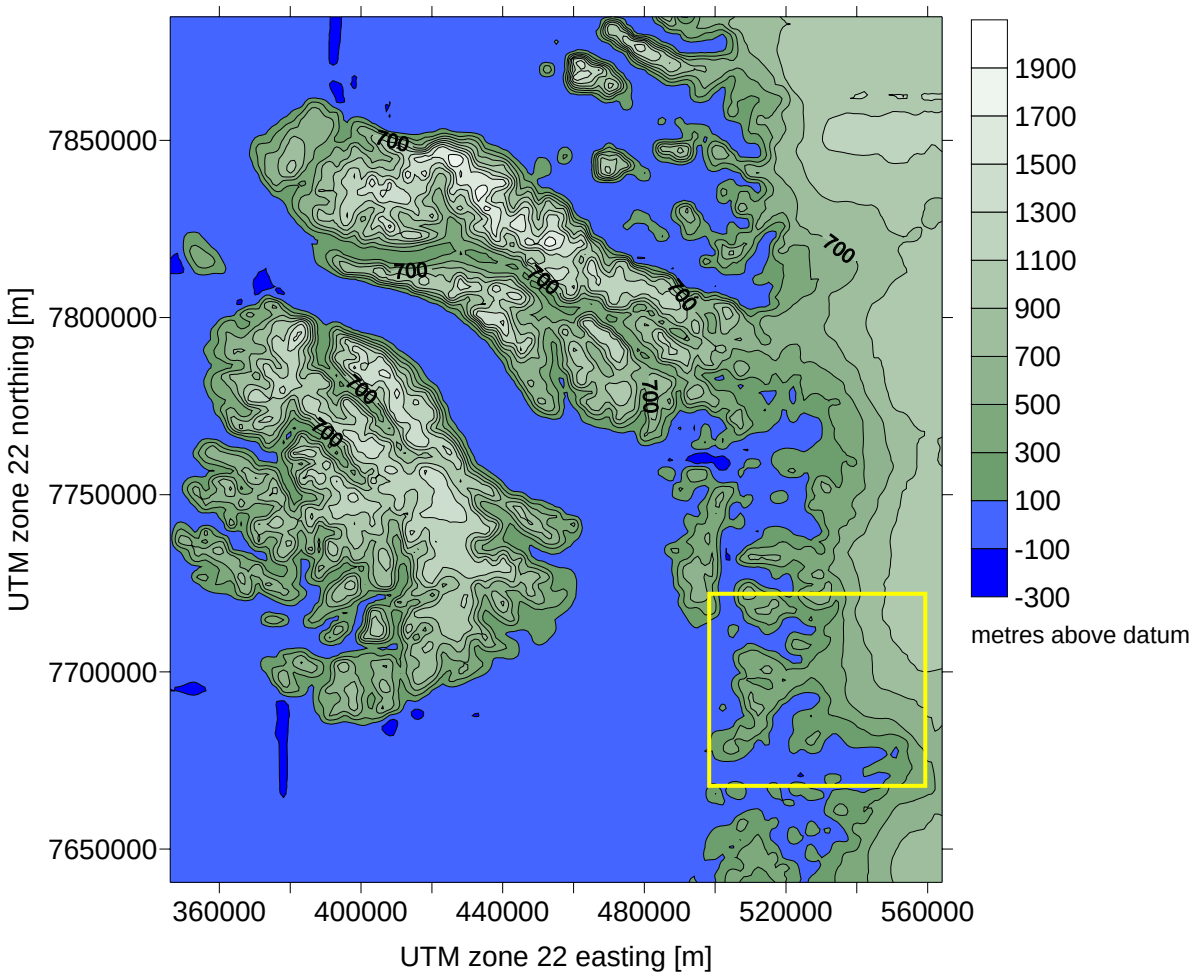

Figure 7: *Surface topography based on aerial photographs taken in 1985, the yellow box delimits the Paakitsoq area (source: GEUS). The map is in UTM22 coordinates (Northing [m] and Easting [m]), datum WGS-84.*

Other work within this project developed an ice-dynamic model of the area to predict the future evolution of the margin based on climate model predictions. For this reason, ice flow lines from the ice divide at the centre to the ice sheet margin are required and the basal elevation model has been merged with a 5 km gridded DTM of the bed of the Greenland ice sheet, based on data from Ekholm (1996). The surface terrain model has similarly also been combined with surface elevation data at a 1 km grid scale also from Ekholm (1996) (see Figures 8 and 9).

The large-scale DEMs were first converted into the same UTM (Universal Transverse Mercator) zone 22 projected coordinate system from polar stereographic coordinates. The latter are often used in Greenland as polar stereographic coordinates give a better shape and size profile with little distortion at high latitudes. The relatively low latitude and small size of the area of interest meant that UTM coordinates were more useful in this study. Unfortunately it

does mean that when looking at output maps related to the ice-dynamic modelling, there is a considerable amount of distortion at the higher latitudes and in areas to the east of the ice divide. This is partly due to the choice of UTM coordinates in general but also especially because we have used an artificially enlarged UTM zone 22 for this study. This is a cosmetic distortion in the output however, and has not affected the results of the modelling process.

After transformation, the large scale DEMs were merged with and then scaled to the local detailed DEMs to produce a surface DEM and a basal DEM of the whole region at a 1 km scale up to the centre of the ice sheet. In order to avoid substantial discontinuities resulting from merging DEMs of different scales, the kriging algorithms developed for the Paakitsoq area were also applied to the large scale DEMs. It should be noted that although the scaling of the large scale DEMs was brought down to 1 km grid squares, the originals were at a scale of 6 km grid squares and inevitably there is a corresponding lack of detailed topography as Figures 8 and 9 show.

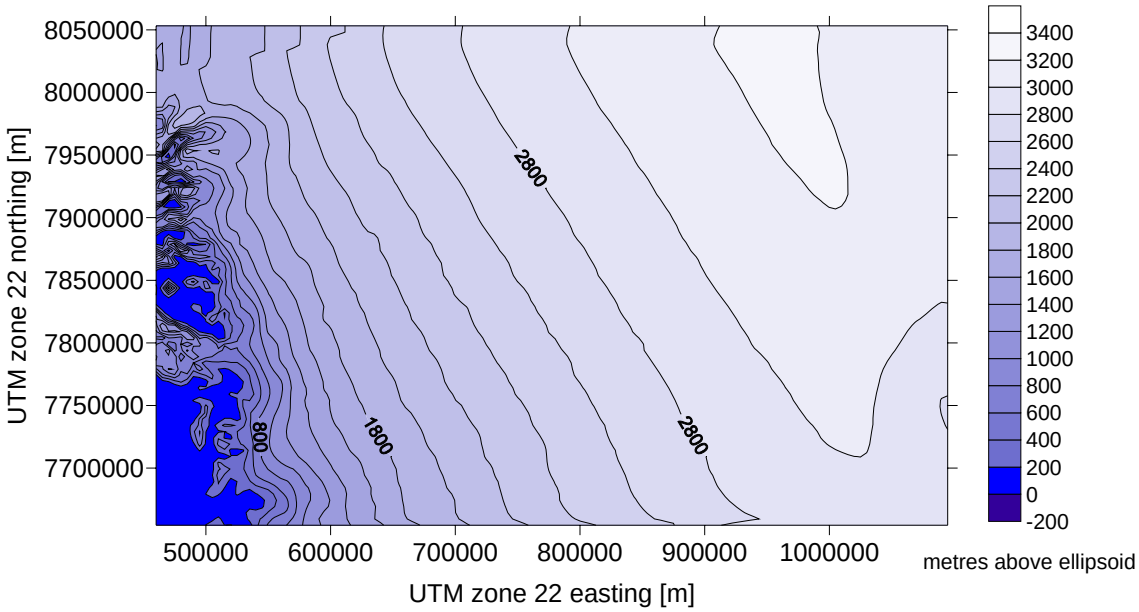

Figure 8. *Surface DEM based on Ekholm (1996). The map is in UTM22 coordinates (Northing [m] and Easting [m]), datum WGS-84.*

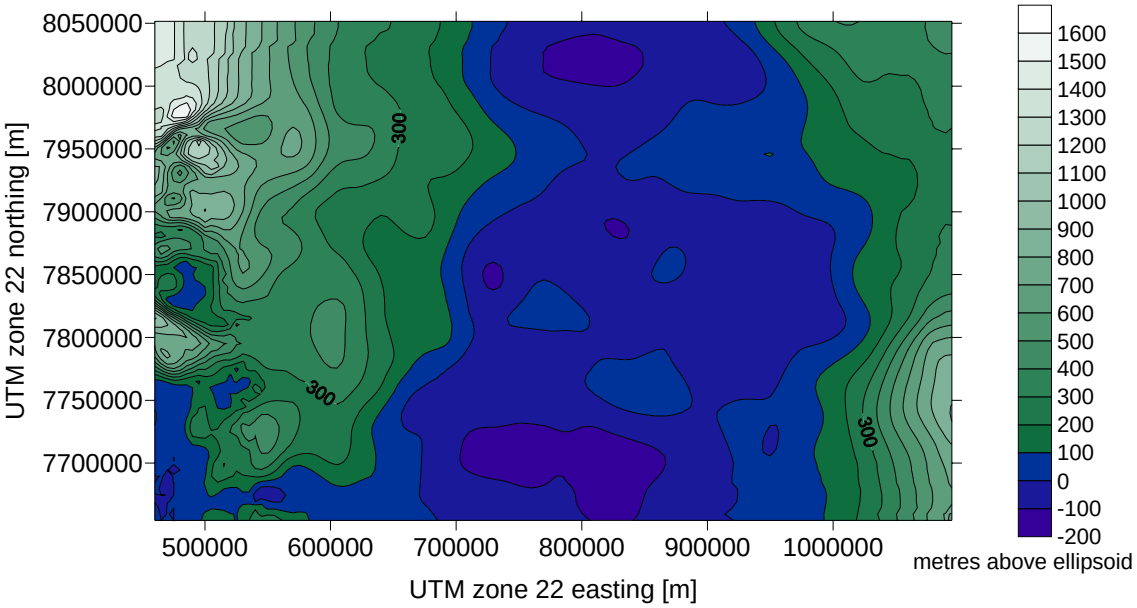

Figure 9. *Subglacial DEM based on Ekholm (1996). The map is in UTM22 coordinates (Northing [m] and Easting [m]), datum WGS-84.*

2.3 Initial Surface Hydrology

As an initial check on the surfaces created using the transformations and kriging algorithms, a preliminary surface basin analysis was carried out with a Rivertools© model applied to the Paakitsoq area alone. The resulting output is presented in Figure 10 and was compared with the aerial photographs and map produced from 1985 data (Thomsen and others, 1988) showing drainage basins and the location of moulins, meltwater lakes and areas of crevassing.

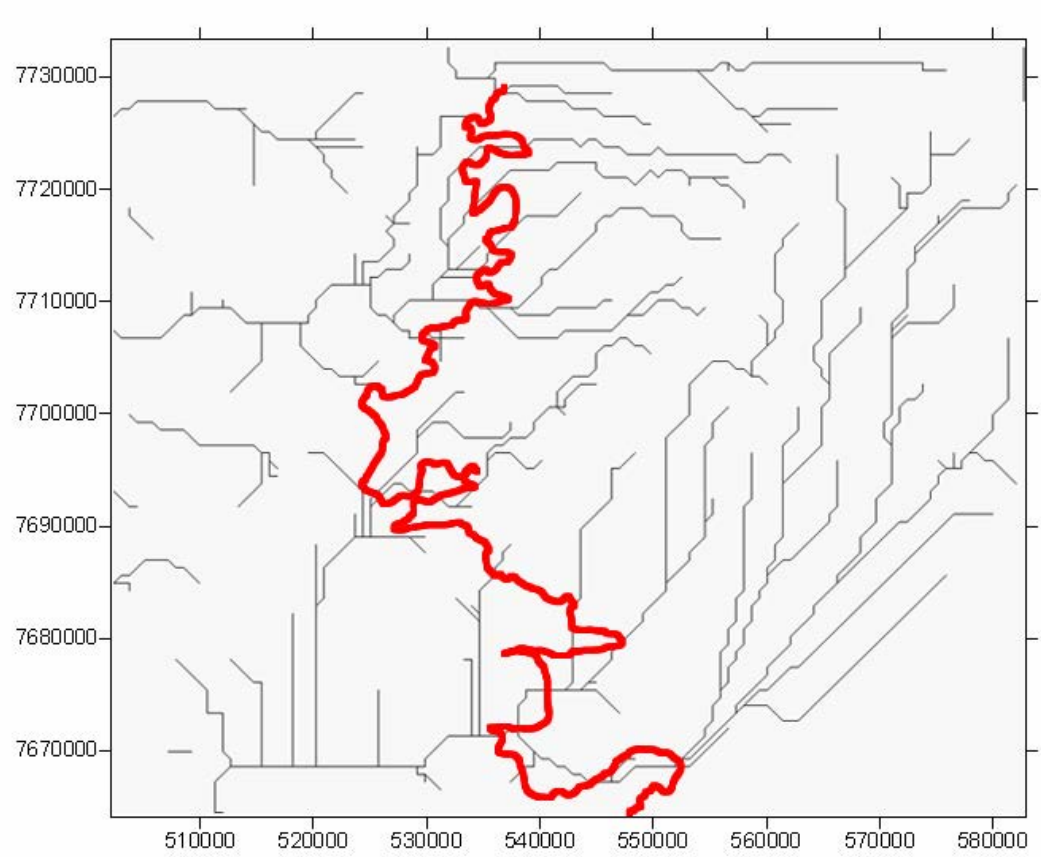

Figure 10. *Drainage basin analysis for the modelled surface, based on the DEMs created from radar and lidar data for the Paakitsoq area. The red line indicates the glacier terminus, taken from the GEUS DEM of the area and based on aerial photos from 1985. The map is in UTM22 coordinates (Northing [m] and Easting [m]), datum WGS-84.*

The surface run-off in the Paakitsoq area predicted by this initial analysis (Figure 10) shows a strong bi-directional trend. To the east, the influence of the Jakobshavn basin is seen, with the predicted surface meltwater streams running from north to south, reflecting the surface contours shown in Figure 4. The rest of the area shows an east to west surface drainage pattern, consistent with ice flow from the ice divide westward to the margin. Aerial photographs were not taken during this field campaign but the predicted drainage pattern based on surface contours is supported by comparison with a map and aerial photographs presented by Thomsen and others (1986). A key difference between the two is the absence in Figure 10 of moulins and melt ponds; these are explicitly excluded in the current model. Research by Zwally and others (2002) shows these to be of primary importance in short term velocity fluctuations in this area and satellite imagery also clearly shows both features to be well developed in the region.

3. Climate Modelling

Perhaps the most important component of evaluating the potential for hydropower is the predicted climate over the next eighty years. The climate determines both the amount of meltwater produced and also how the ice-sheet margin will flow and evolve in response to climatic variability. A further complicating factor is predicting how climate will change in response to anthropogenic forcing. To investigate this, output from the Danish Meteorologi-

cal Institute's (DMI) regional climate model, HIRLAM, nested in a global circulation model, ECHAM4 was used.

3.1 Climate Model Summary

The climate scenario used in the climate model is the IPCC SRES B2 scenario. It was published in the Special Report on Emission Scenarios by the Intergovernmental Panel for Climate Change (Nakicenovic & Swart, 2000) along with three other main scenarios (A1, A2 and B1) and was intended for use in the IPCC third assessment report, published in 2001. The B2 scenario was chosen as it is relatively conservative, with the term 'medium' assigned to the all the following parameters: 'Population growth', 'GDP growth', 'Energy use', 'Land-use changes', 'Resource availability' and 'Pace of technological change'. It is described in the SRES as follows: 'The B2 storyline and scenario family describes a world in which the emphasis is on local solutions to economic, social, and environmental sustainability. It is a world with moderate population growth, intermediate levels of economic development, and less rapid and more diverse technological change than in the B1 and A1 storylines. While the scenario is also oriented toward environmental protection and social equity, it focuses on local and regional levels.' The SRES scenarios have been criticised as being too optimistic, in particular about the development of environmental technologies. However, the SRES scenarios remain useful by providing a common ground for making predictions of climate-induced change.

The predictions based on the different scenarios are shown in Figure 11. The aim of nesting the regional climate model, HIRLAM, in the global circulation model, ECHAM4 was to deliver high-resolution (25 km by 25 km grid) regional climate predictions for Greenland. The combined model has been given the name HIRHAM4 and is among the most advanced of its kind. A transient run of HIRHAM4 covering from 1950 and up to 2080 produced the 2 m air temperatures and precipitation fields necessary to force our mass balance model.

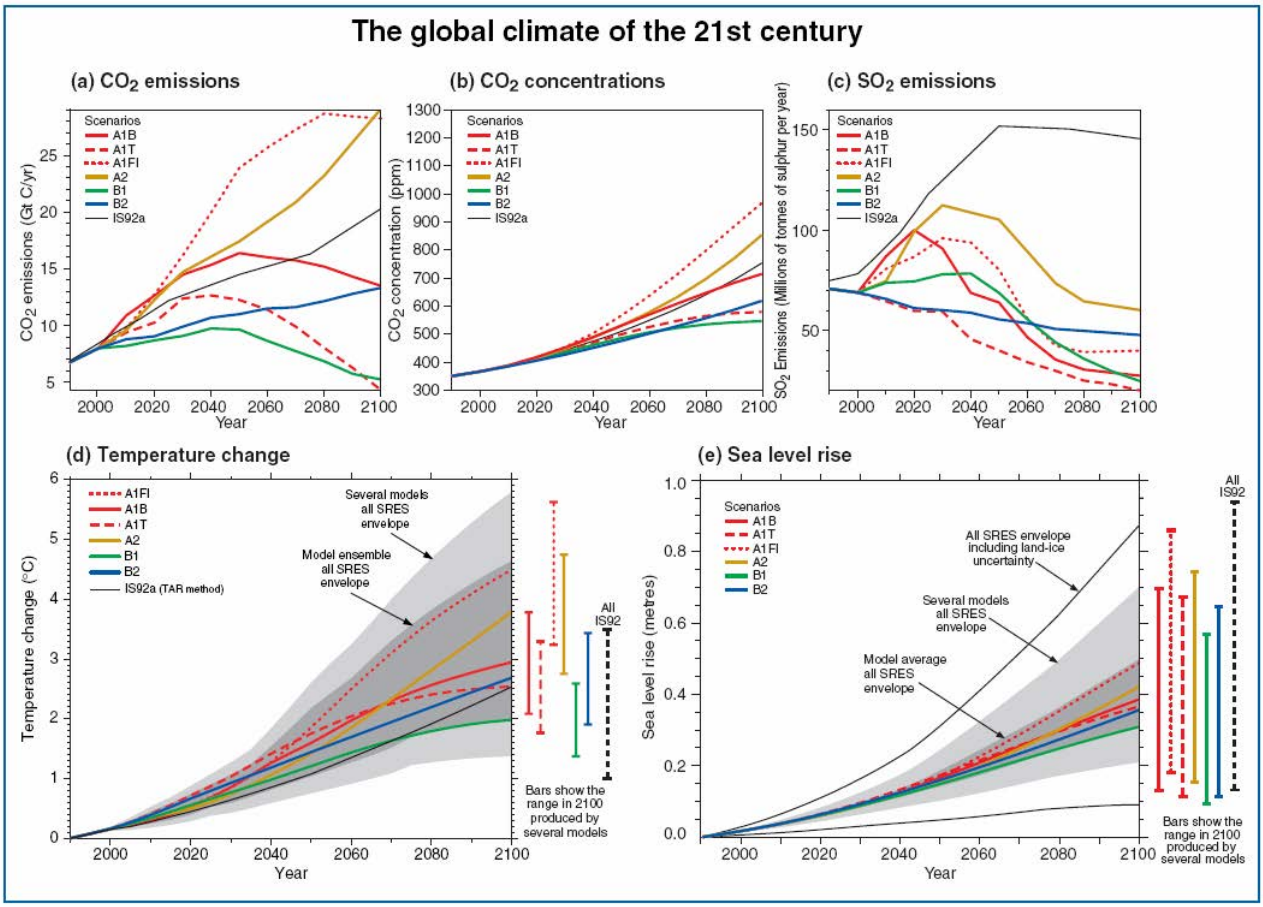

Figure 11. *Summary of the changes expected under the 4 different scenarios from the 2001 IPCC Working Group I technical report (Nakicenovic & Swart, 2000, 2001).*

The climatic output data was used for two purposes, in the first instance to drive the dynamic changes of the ice sheet, and in the second to predict rates of melt and run-off. This required substantial processing of the output.

3.2 Downscaling of the climate model output

The initial 25 km gridded output required interpolating to be useful on the catchment scale of this study. The HIRHAM4 output was therefore downscaled to our finer grid resolution (250 m by 250 m catchment scale grid) and calibrated to the air temperature and snow accumulation measured on the actual ice-sheet margin. A detailed account of the procedure used is given in Appendix B, but a summary is given here.

Scaling of the output is required to take into account the topographic effect on temperature and precipitation. In particular, the ice sheet surface elevation is not well defined in the DMI model, and a lapse-rate correction is necessary to account for topographic variability. Lapse rates describe how temperature changes with elevation and were applied to gridded topography, which were then used to recalculate the scaled climate data. The HIRHAM4 model was not designed to model individual years, but rather catch the overall climate dynamics. It was therefore not feasible to compare model output and observations for specific years. Instead, we compared mean values over the entire period of the observations. Observations of air temperature and snow accumulation are available from five automatic

weather stations on the ice sheet margin in the region, forming a part of the US Greenland Climate Network (GC-Net). These data have been collected from 1995 to present and were reduced to monthly means to facilitate a comparison.

As the ice sheet surface itself can never exceed beyond the melting point, it exerts a cooling effect on the surface boundary-layer of the atmosphere during large parts of the summer. This means that temperature lapse-rates can be very different depending on the season, and also that standard values from non-ice-sheet locations can not be used. Thus, the observed air temperature series were used to establish the monthly temperature lapse rate on the ice sheet. Lapse rates calculated by Steffen and Box (2003) at Swiss Camp were initially used to scale output. Their values are given in Table 1.

Jan	Feb	Mar	Apr	May	Jun	Jul	Aug	Sep	Oct	Nov	Dec
0.65	0.86	0.77	0.61	0.54	0.51	0.50	0.53	0.67	0.75	0.94	0.88

Table 1 *Monthly lapse rates (ºC/100m) on the Southwest Greenland ice sheet, (Steffen and Box, 2001, Fig. 8).*

The elevation difference between the coarse DEM of the HIRHAM4 model and the detailed high-resolution DEM available for the Paakitsoq region was determined. Using this known elevation difference, the HIRHAM4 output was lapse-rate corrected to the high-resolution catchment scale, effectively downscaling the air temperature predictions on a monthly basis. As the HIRHAM4 model is not well suited to capture the atmospheric boundary-layer peculiarities of an ice sheet surface, an additional correction was performed. The correction consisted of comparison of the mean monthly modelled and downscaled temperature fields with mean monthly observed temperatures over the entire observation period. This made it possible to establish a monthly correction scheme as a piece-wise linear function of elevation on the ice sheet. Subsequently, this temperature correction scheme was applied to the entire HIRHAM4 model output series spanning 1950 to 2080. These additional corrections are shown in Table 2.

Month	0 – 1200 m	1200 – 2000 m	2000 – 3000 m
January	0.0092Z - 7.533	-0.0007Z + 4.3567	-0.003Z + 8.8701
February	0.0139Z - 13.522	0.005Z - 2.8552	-0.0071Z + 21.434
March	0.0071Z - 3.3473	0.0036Z + 0.8298	-0.008Z + 24.089
April	0.0002Z + 2.7756	0.0012Z + 1.5917	-0.004Z + 11.975
May	-0.0018Z + 6.789	-0.003Z + 8.2039	-0.0022Z + 6.6117
June	-0.0037Z + 7.2144	-0.0027Z + 6.0347	-0.0006Z + 1.9041
July	-0.0054Z + 8.5765	-0.0012Z + 3.4916	-0.0011Z + 3.2748
August	-0.0017Z + 3.0843	-0.0021Z + 3.6071	0.0006Z - 1.7787
September	0.0039Z - 3.8359	-3E-06Z + 0.8476	-0.0008Z + 2.3628
October	0.0054Z - 5.4259	0.0034Z - 3.024	-0.0038Z + 11.328
November	0.0055Z - 6.358	0.0064Z - 7.406	-0.0054Z + 16.182
December	0.0063Z - 8.9578	0.0035Z - 5.6419	-0.0014Z + 4.0743

Table 2. *Additional temperature corrections applied to mean monthly temperatures after the lapse-rate correction. Each correction function was calculated using a piece-wise linear function, where Z is the elevation. Three different functions were applied based on the elevation of the calibration measurement stations. Above 3000 m the output was assumed to be correct and no additional correction was applied.*

Similarly, precipitation from the HIRHAM4 model was compared to snow accumulation measured at the US automatic weather stations (AWS). Actual precipitation gauges are notoriously poor at collecting snow precipitation, especially in windy conditions. A more robust measurement of snow height from the AWS was used, employing an assumed fixed mean snow density of 380 kg/m^3. The snow density value was taken from a 10-year study at the Amitsuloq ice cap (Ahlstrøm and others, 2007). The comparison showed that the modelled precipitation was only half of the observed precipitation in the Paakitsoq region. Consequently, the entire model output series were corrected to twice the amount of precipitation. Both the near-surface temperature and the precipitation corrections were substantial and calls for caution in relying too much on the absolute values of the resulting climate parameters. Emphasis should be on the trend of the HIRHAM4 output, rather than on the absolute values.

4. Melt modelling

The downscaled fields of near-surface air temperature and snow accumulation were used to drive a mass-balance model, based on the temperature-index (or degree-day model) method. This type of model exploits the high statistical correction between ice/snow melt and the amount of time the air temperature is above the melting point. Although the concept behind the degree-day model is simple, the procedure was fairly complex and is given in full in Appendix C. The melt model was developed by Reeh (1991) and applied here. It requires as input gridded values for the surface elevation, the mean monthly temperature and the mean monthly precipitation. The model applies a degree-day factor (DDF) to these grids in order to calculate the amount of melt produced. Degree-day factors are constants applied in a simple function (Equation 4) to calculate ablation and must be determined by means of field data:

$$N = \beta T_{pdd} \tag{4}$$

In Equation 4, ablation, N is the product of the sum of all positive daily mean temperatures (in ºC), T_{pdd} and the degree-day factor, β (in millimetres water equivalent per day per Kelvin). The degree-day factors are determined for snow and ice separately due to their significantly different physical properties, notably the surface albedo. The DDF for ice is known to vary with elevation on the western margin of the Greenland ice sheet, due to differences in the surface albedo. This change with elevation was incorporated with values from the literature (Hock, 2003). The DDF for snow was also chosen within published values, but higher than the few values previously determined for the Greenland ice sheet in order to approach the observed discharge. Thus, the choice of the DDF for snow incorporated a degree of model calibration with the observed basin discharge series. The chosen degree-day factors for ice are given in Table 3.

Elevation (m)	*Degree Day Factor (mm per day per ºC)*
All levels - snow	4.5
Ice 0 – 316	7.2
Ice 317 - 1073	Linearly increasing from 7.2 to 20
Ice 1074+	20

Table 3. *Values used for the degree day factors.*

The outputs from the melt model took the form of two grids depicting melt and mass balance across the region. Two examples of these are shown in Figures 12 and 13. The mass balance grids were both summed and averaged over 10 years and both of these were used as input to the ice dynamic model. The melt grids were used as input to the basin delineation model.

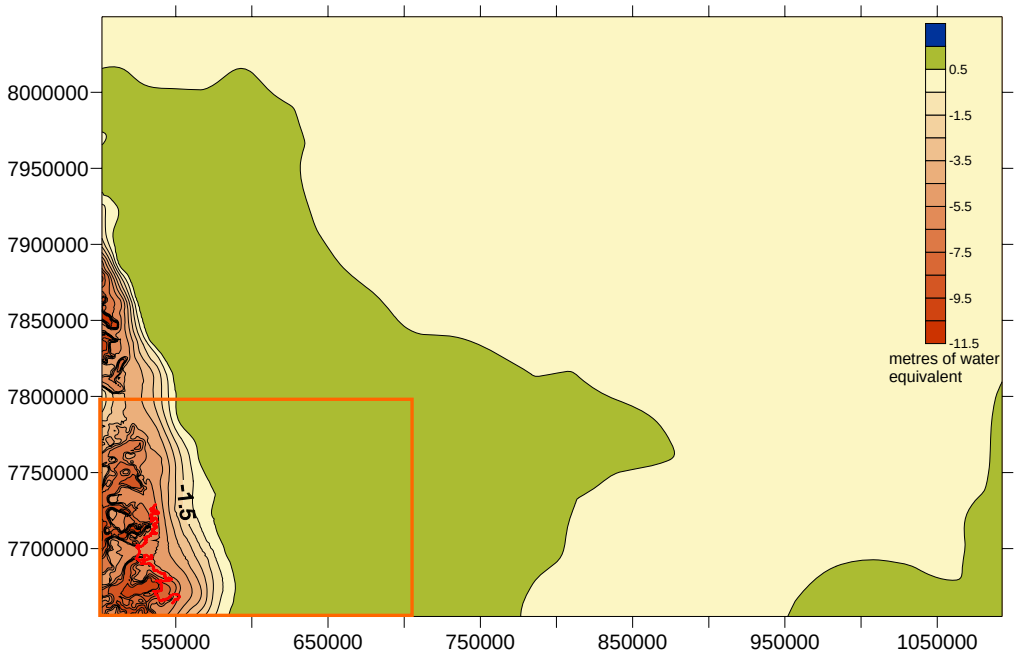

Figure 12. *Map of mass balance for the single year2080. The red line indicates the 2005 ice margin. The units are metres of water equivalent. Note that in the centre of the ice sheet mass balance is close to zero or slightly positive, but at the margins it becomes strongly negative. The orange box shows the Paakitsoq subsection illustrated in Figure 13 below.*

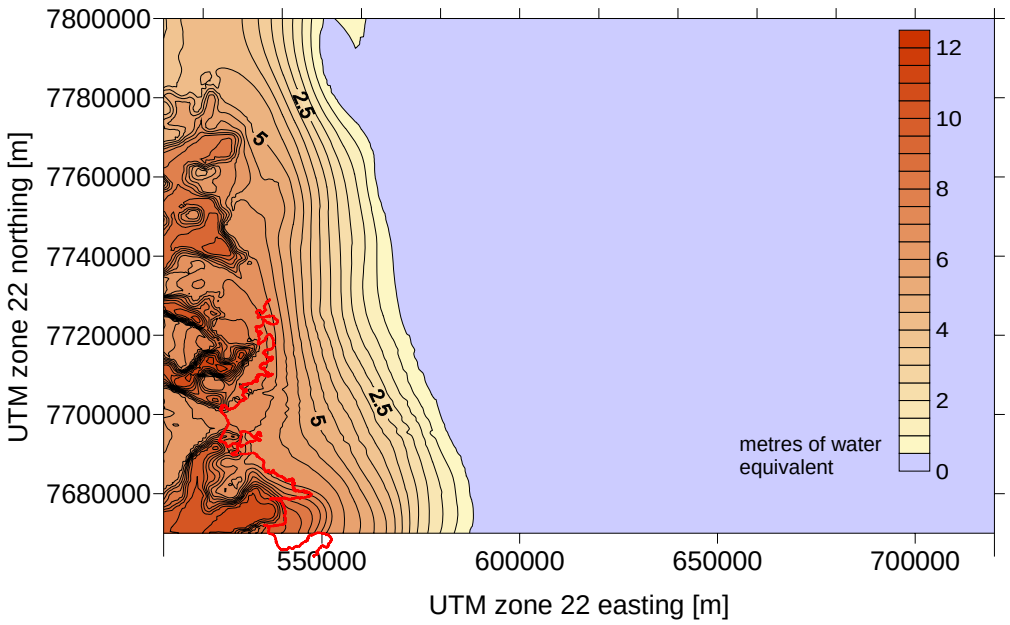

Figure 13. *Map of predicted melt in the year 2080. The majority of the melt is concentrated around the margin. Note that this area is only a subsection of the larger balance map shown above.*

The cumulative mass balance data for 10-year periods are interesting results in themselves as they indicate the broad trend of the climate data and how the surface may be expected to respond. The plot in Figure 14 shows part of a profile slice through eight average mass-balance grids. The plotted profile is the same as the flow line profile used to determine dynamic elevation changes and so is directly comparable with the flow line profiles presented in Section 5.

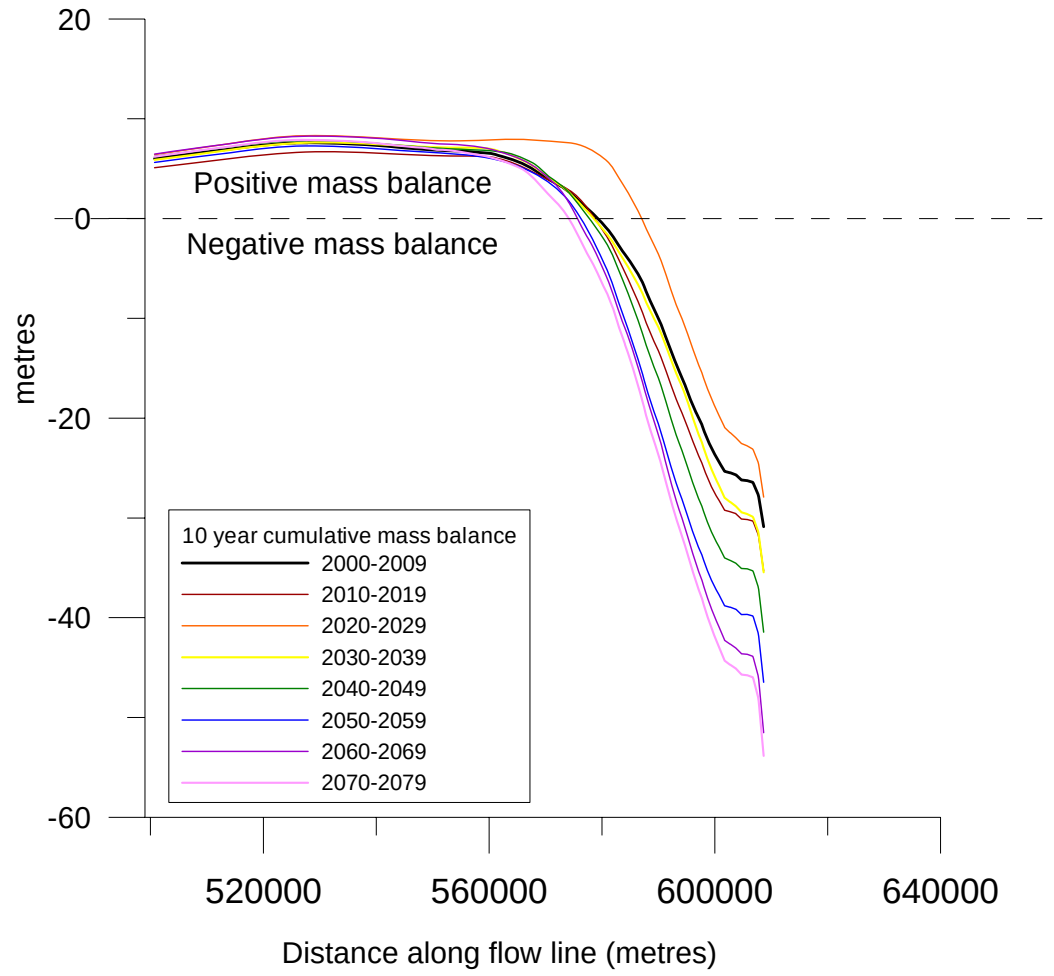

Figure 14. *Mass balance trend 2005-2080 along a flow line, ,for clarity this graph shows only the part closest to the margin. Further back towards the centre, the trend is very similar to the 2000-2009 reference period.*

When interpreting Figure 14, it is important to remember that these are indicators of the variability and trend, rather than a specific prediction for a specific period. Note the higher mass gain and lower ablation rates during the period 2020-29 for instance. This will have a significant effect on the ice sheet surface. Later profiles, after 2040 show a steepening gradient with a small amount of extra accumulation higher up and increased ablation lower down. The general pattern is one of initially continuing retreat with a significant increase predicted in the later half of the century.

5. Ice dynamics

Ice dynamics refers to processes relating to the flow of ice. The dynamics of an ice sheet result from the balance between accumulation through snowfall, usually at the centre of the ice sheet, and the loss of mass due to melting or iceberg calving at lower levels closer to the margins. Driven by gravity, ice flows slowly outwards from areas of accumulation to areas of ablation (mass loss). If the amount of snowfall or melt changes then the rate of ice flow will also change, along with the surface elevation and geometry of the ice sheet, with a consequent change to the surface and to drainage patterns. Even if there is no climatic change failing to include ice dynamics, which bring ice to lower elevations to replace losses due to melt, will result in unrealistic predictions of changes to the ice margin. Therefore, when modelling ice sheet changes over longer time periods, and especially given predicted climatic changes, the dynamics of ice flow must be taken into account.

The ice-dynamic model used for this purpose was developed by Reeh (1988) and uses both the standard Fortran programming language and surfer gridding software. It was modified and updated for the purpose of this project and run in five year increments. The input data to the model consists of eight geographical grids (Figure 15 a-h):

1. Surface elevation
2. Bed elevation
3. Mass balance (averaged over 10 years)
4. Basal ice temperature
5. Surface ice temperature
6. Depth of the transition between Weichselian and Holocene age ice
7. Curvature of the surface contours
8. Slope aspect of the surface terrain

Since the material properties of ice are dependent on temperature and pressure, data on surface and basal topography and ice thickness are crucial. Other corrections are incorporated in the model to account for the basal and surface temperature of the ice and the vertical transition between older and colder Weichselian age ice (ca. 20,000 years ago) and younger warmer Holocene age ice (ca. 12,000 years old), which have different flow properties. The model does not include the effects of sliding on the bed. This is known to occur in some places areas close to the margin, however for the majority of the area in this study, it is not a relevant process. Recent measurements within the ice sheet basin indicate that sliding is only a small component of the overall velocity, although it does contribute to significant and often short term velocity fluctuations in the summer as a result of meltwater lakes draining to the bed (Joughin and others, 2008).

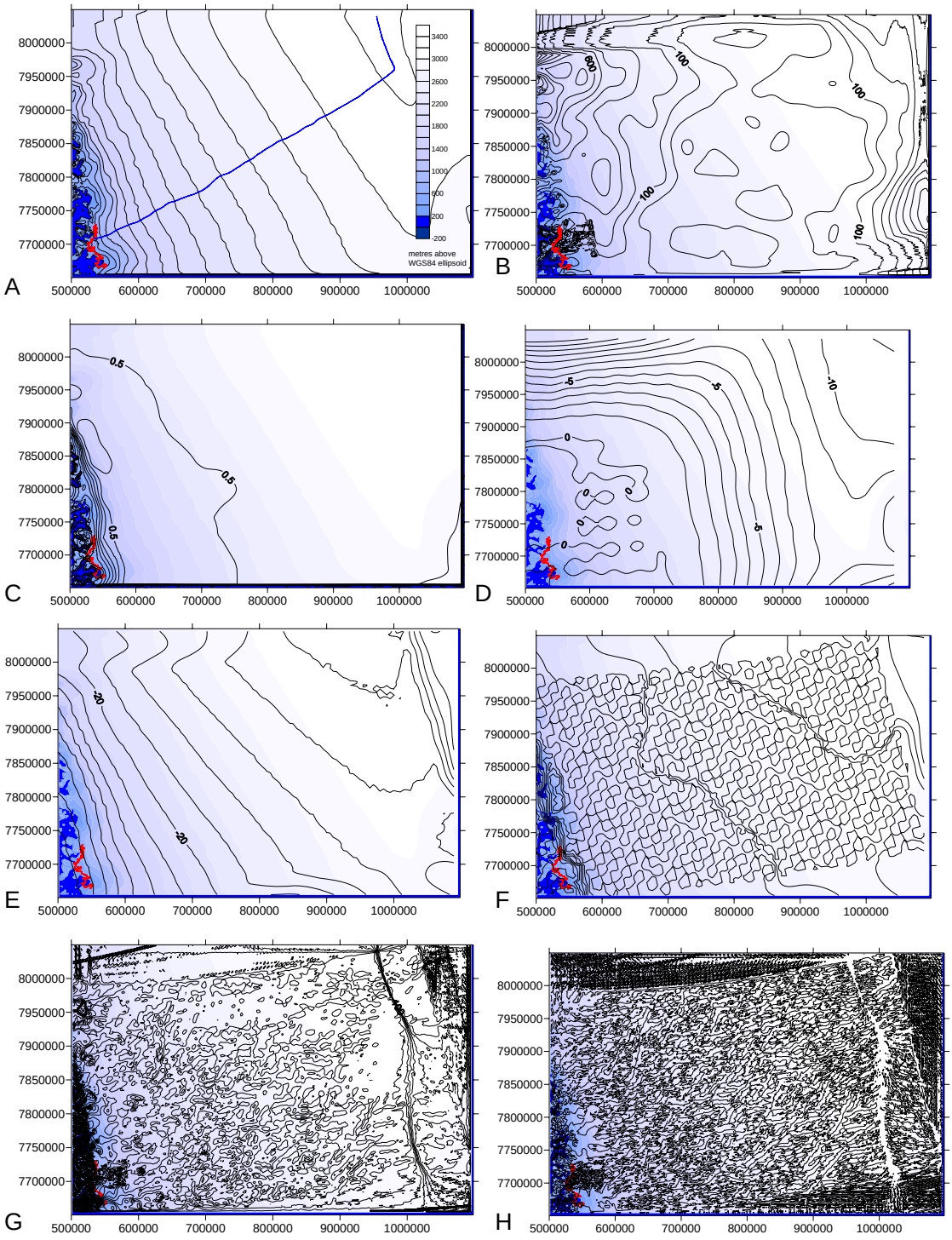

Figure 15 a- h. *The initial gridded starting values for the model. The eight grids described in the text are: a) Surface elevation in 2005; b) Basal elevation; c) Average mass balance from 2000-2004; d)Basal ice temperature; e) Surface ice temperature; f) Depth of transition between Holocene and Weichselian ice; g) Plan curvature of the surface; h) Slope aspect of the surface. Note that all gridded values have been laid over the surface elevation contours to show how the values relate to the elevation, all grids are in UTM zone 22 coordinates. The red line in all images is the 1985 ice margin line.*

The full procedure is outlined in Appendix D, and the model is described in depth in Reeh (1988), but a summary is given here. The first part of the model calculates the location and direction of the flow line from any point at the margin to the centre of the ice sheet, based

on surface and basal topography. The flow line used in this study is shown in Figure 16. The slice function is used within surfer to extract the values from each of the eight grids along this flow line. These values are used within the second part of the fortran model to calculate the full strain rates, stresses and velocities in three dimensions at 1 km intervals along the flow line. The calculations are also performed vertically at each point at regularly spaced depths, the values of which will be determined by the ice thickness. The model is two-dimensional but uses the surface curvature to incorporate a term for flow divergence or convergence, in order to calculate the transverse to flow values. This is based on a sound physical understanding of the material properties of ice and is a good compromise between detailed understanding of the physics at a high resolution and processor calculation time. The third and final part of the fortran model predicts the surface elevation of the flow line, and the ice thickness based on the given mass balance for the 10 year period.

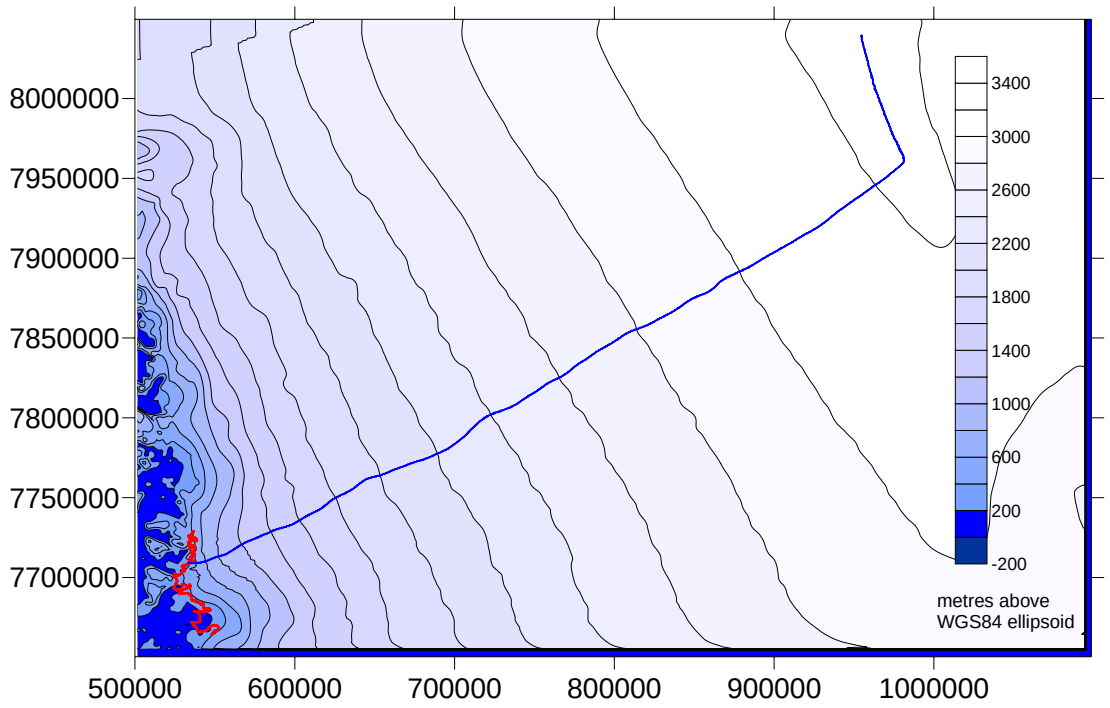

Figure 16. *The flow line (in blue) used in this study, extending from the ice divide to the ice sheet margin (shown in red). Elevation contours are in metres and the map coordinates are Easting (m) and Northing (m) UTM zone 22. The map datum is WGS84.*

The aim of the modelling was to gauge the trend of ice margin changes as well as the likely magnitude. For this reason, the simple procedure outlined above was repeated twice for each ten-year period. The initial run used the initial surface elevation based on the lidar data set. The second run used a different elevation grid, calculated from the static elevation change (the difference in cumulative mass balance between two subsequent decades) and the initial elevation grid (see Appendix D). This process indicates how much change would be expected given no ice flow at all, and is therefore known as the static elevation change, rather than the dynamic elevation change. Based on the static change, the second model run predicts how the ice dynamics will respond to a given mass balance (and by extension the climate averaged over 10 years).

The difference between the surface elevations predicted in the first model run and the second model run were used to calculate the total surface elevation change (both dynamic and static). The predicted surface elevation change along the flow line profile was used to define a 7th order polynomial (Figure 17) in Grapher© which could then be applied across the surface in order to extrapolate the calculated surface change across the ice sheet.

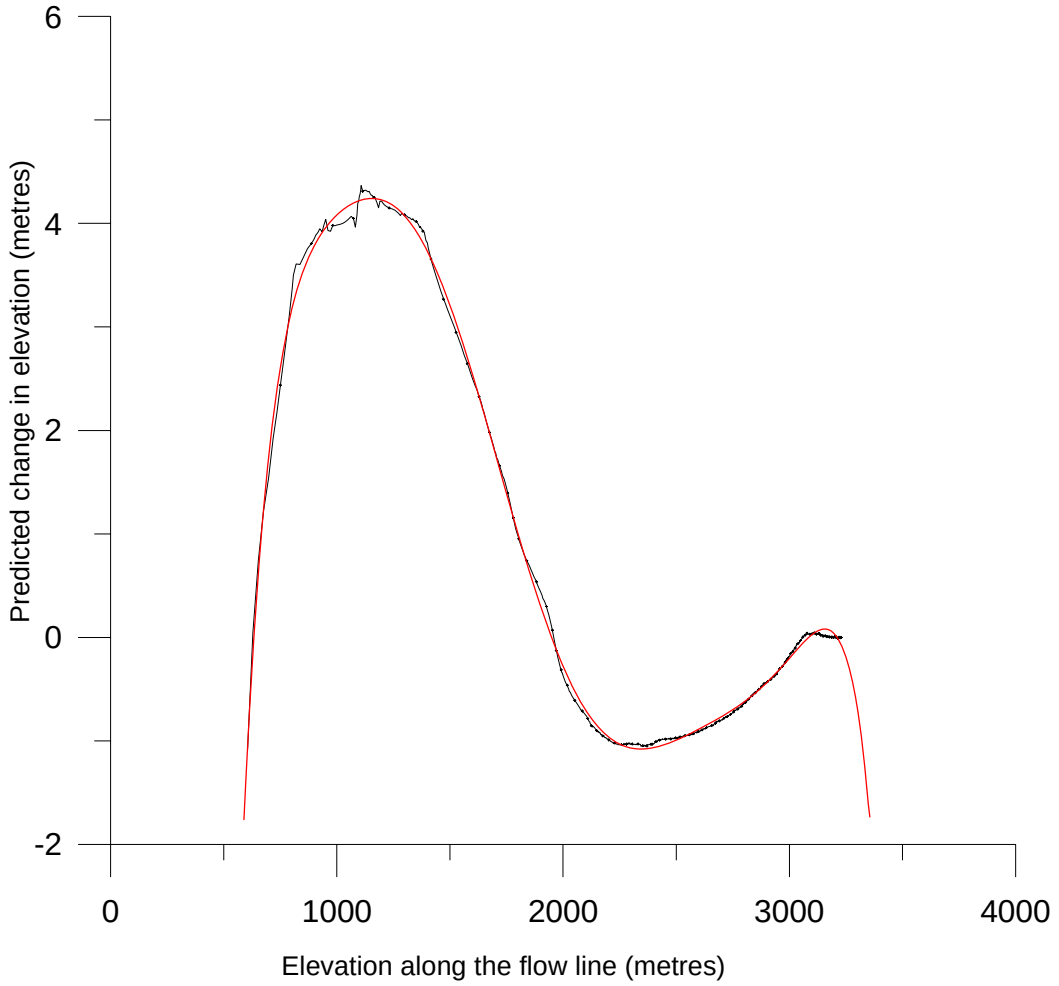

Figure 17. *Example of a polynomial function (red line) approximated to the calculated surface elevation change (black line). In this case, the data are for surface changes between 2000 and 2009.*

Generalising the elevation change from the flow line across the ice surface is particularly necessary, as surface curvature is used in the model to take into account flow divergence and convergence. If only the elevation change along the flow line is taken into account the surface curvature is artificially altered, giving skewed results in subsequent iterations. The output surface altered, with the extrapolated function of each increment, was used to initialise the input surface for the following model run. Figure 18 below shows the development of the surface profile at 10-year intervals.

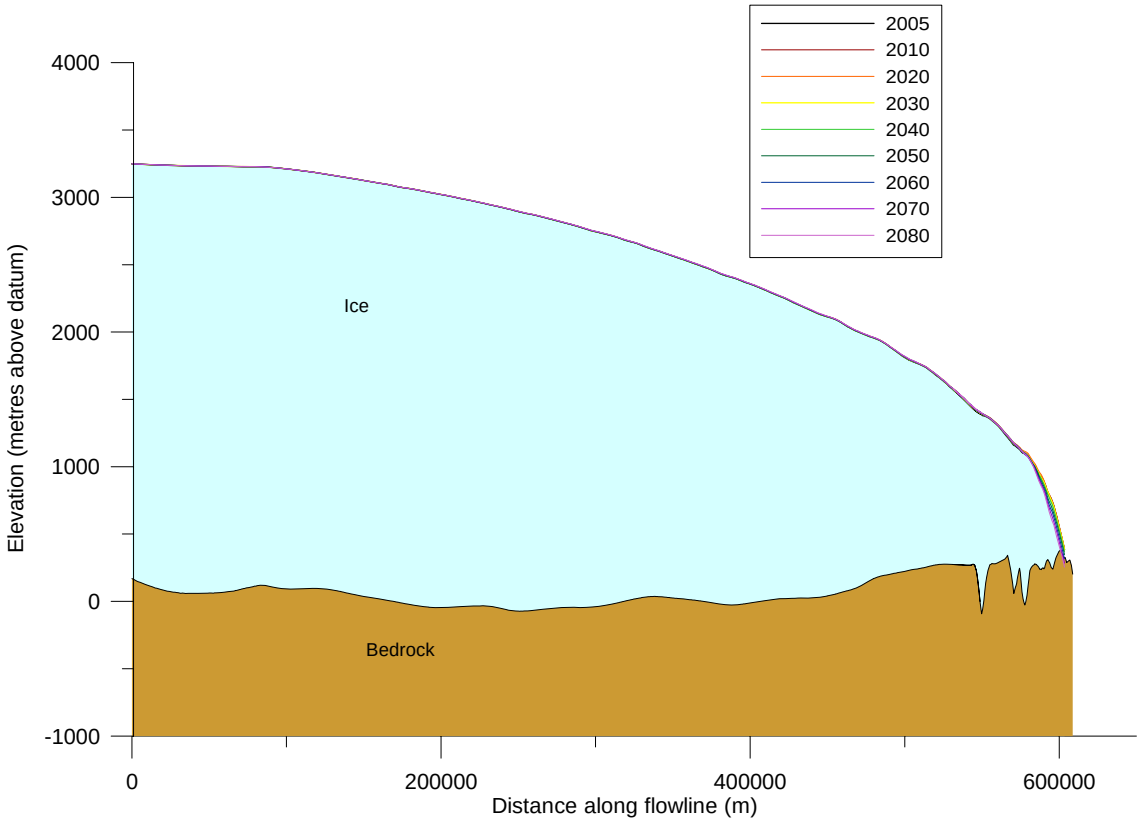

Figure 18. *Modelled surface elevation profiles along the central flow line of the basin from 2005 to 2080 at 10 year intervals. Elevation (y-axis) is in metres above the ellipsoid and distance (x-axis) is in metres from the ice divide.*

Figure 18 summarises the main changes in surface elevation along the full flowline (see Figure 16). As the main changes are difficult to track, Figures 19 and 20 display the surface profiles for the Paakitsoq area in more detail. Note that most of the changes are concentrated around the margin, corresponding to the steeper gradient in mass-balance changes at this location. The mass-balance profile in Figure 14 explains the trend of these changes and shows that the magnitude of the surface elevation change is mainly down to static (i.e. mass balance driven) change with dynamic processes mainly operating to replace mass. The rate of surface lowering is expected to remain consistent with the 1 metre per year measured by previous studies in this area.

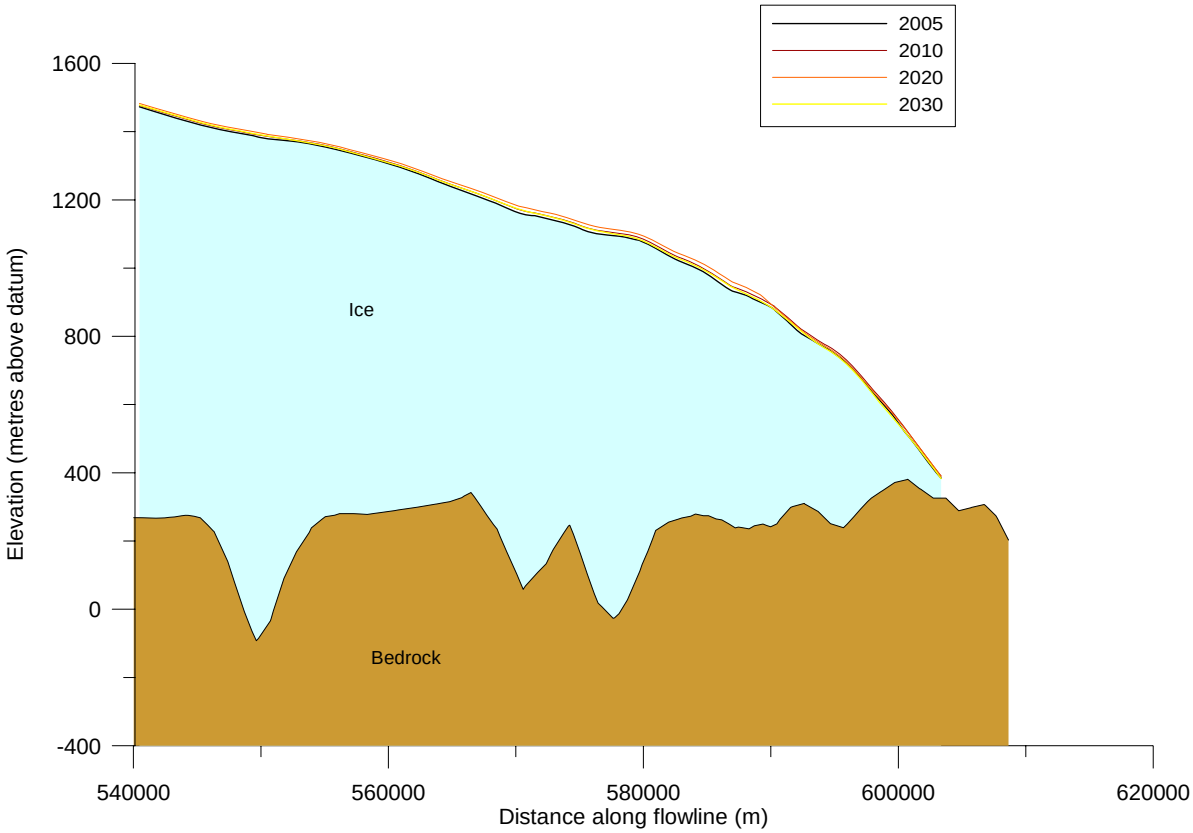

Figure 19. *The Paakitsoq area of the margin showing the profile changes up to the year 2030. Elevation (y-axis) is in metres above the ellipsoid and distance (x-axis) is in metres from the ice divide.*

The early part of the century shows the ice sheet remaining very similar in terms of surface elevation, with a slight increase of the ice sheet, particularly higher up. The mass-balance profiles illustrated in Figure 14 show a fairly consistent picture of mass balance being very similar to present day values for the first two decades with a much higher modelled accumulation and reduced ablation in the years 2020-2029.

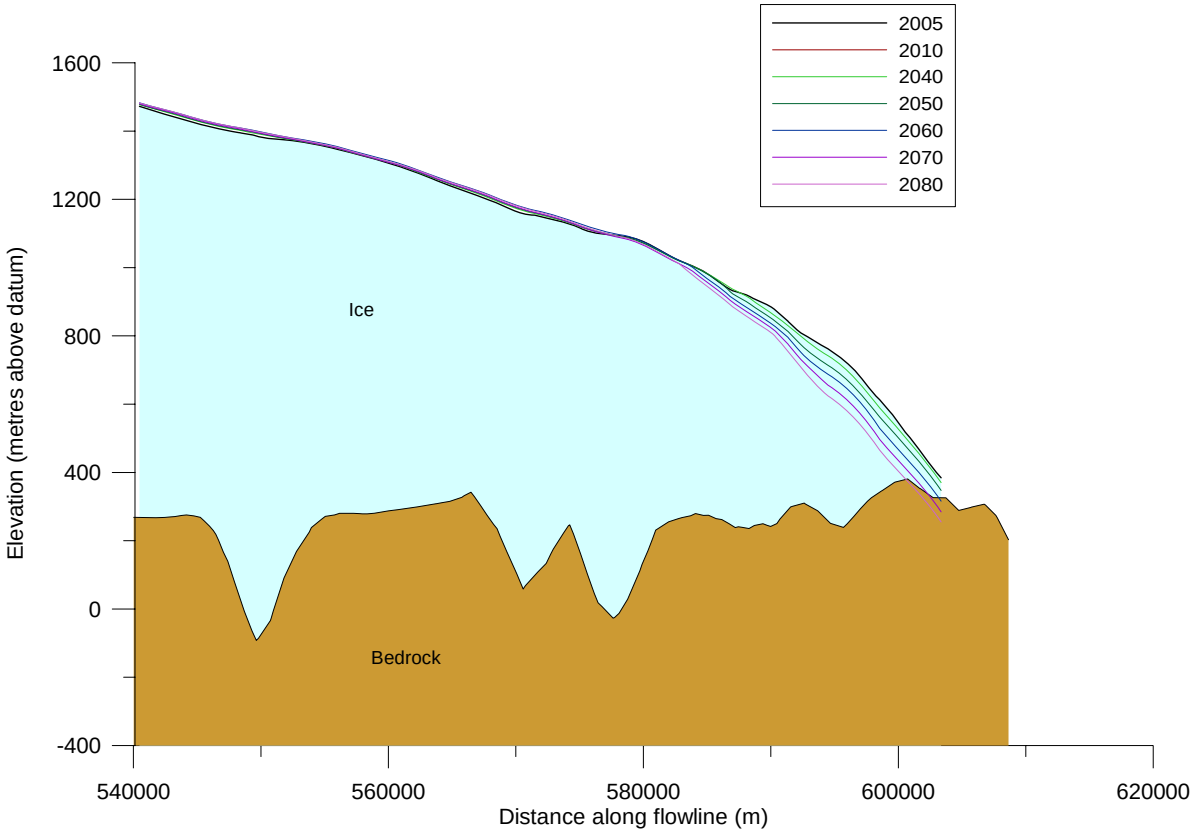

Figure 20. *The Paakitsoq area of the margin showing the profile changes from the years 2030 to 2080. Elevation (y-axis) is in metres above the ellipsoid and distance (x-axis) is in metres from the ice divide.*

In the latter part of the century (from 2040 onwards), the mass-balance gradients become steeper and the ice sheet responds to this with a steepening of the profile close to the margin. The surface outputs from the dynamic model were used to determine the drainage surfaces at 10 year intervals. These are presented in the next section. They were not used as an input into rescaling the climatic output. Given the relatively small surface change predicted, this is not expected to be a major source of error.

6. Drainage Basin and Discharge Analysis

The final part of the project required modelling to delineate drainage basins and predict meltwater discharge into the lakes. The output surfaces from the dynamic model produced at 10 year intervals were used as input to the basin delineation model. Delineation of hydrological ice sheet drainage basins is complicated because the watershed is not simply defined by the surface drainage, but must include a formulation of the englacial water routing as shown by Shreve (1972). This formulation is simplified by the assumption of Björnsson (1982) that all meltwater reaches the bedrock through moulins and crevasses and drains along the base of the ice sheet which is assumed to be impermeable. This is a reasonable assumption for large scale flow in regions with basal ice near the pressure-melting point and has been applied by for example, Thomsen and others (1988), Hagen and others (2000) and Ahlstrøm and others (2002). Recent observations on the western margin of the Greenland ice sheet by Das and others (2008) has proven that surface meltwater can

penetrate 1 km of cold ice (ie. Ice at subfreezing temperature). Das and others (2008) observed how a large surface meltwater lake drained catastrophically to the basal drainage system through cracks formed by filling existing crevasses with meltwater from the lake. The weight and melting capacity of the meltwater from the lake caused the crack to penetrate all the way to the bed, a process that has previously been proven to be theoretically possible. The Paakitsoq region resembles the study area of Das and others (2008) and is known to be drained by a well-developed network of surface streams feeding into local moulins (Thomsen and others, 1988). The application of a simplified model assuming instant meltwater transport to the bed through thick, cold ice is therefore justified by observations. The simplified model implies that the direction of the water flow at the base of the glacier is determined by a water pressure potential Φ_b, given by (5):

$$\Phi_b = \rho_w g Z_b + k\rho_i g\left(Z_S - Z_b\right) \quad (5)$$

where ρ_w and ρ_i are the densities of water and ice, respectively, Z_b is the bedrock elevation, Z_s the elevation of the ice sheet surface and g the gravitational acceleration. The last term in the equation is the subglacial water pressure which is proportional to the pressure of the overlying ice with the factor *k*, ranging from *k = 0* corresponding to atmospheric pressure in subglacial channels to *k = 1* for the situation where the subglacial water pressure equals the overburden pressure exerted by the ice. The water at the base of the glacier will flow in the direction of the maximum gradient of the water pressure potential. Basin delineation and a drainage pattern was then calculated from the potential surface by the hydrological software package RiverTools©. Thus, this model predicts, based on surface and subglacial topography, the direction of the flow of water beneath the ice. Sub-glacial drainage is important as it forms the bulk of the run-off water entering into the lakes.

Measurements in boreholes drilled through the ice near the ice-sheet margin within the basin late in the melt season, points at basal water pressures ranging between 79% and 105% of the ice overburden pressure, corresponding to a value of the k-factor between 0.79 and 1.05 (Ahlstrøm, 2007). The figures presented in this section show the drainage basins for three values of the k-factor, 0.5, 0.7 and 0.9. They are presented in decadal intervals and given separately as a combined drainage area for all of the lakes, and as a drainage area for lake 233 alone. Analysis shows that the meltwater discharge is divided fairly even between the sub-basin draining to Lake 233 and the sub-basin draining straight to Lakes 326 and 187. For lower values of the k-factor, the sub-basin draining to Lake 233 becomes the dominating source of meltwater.

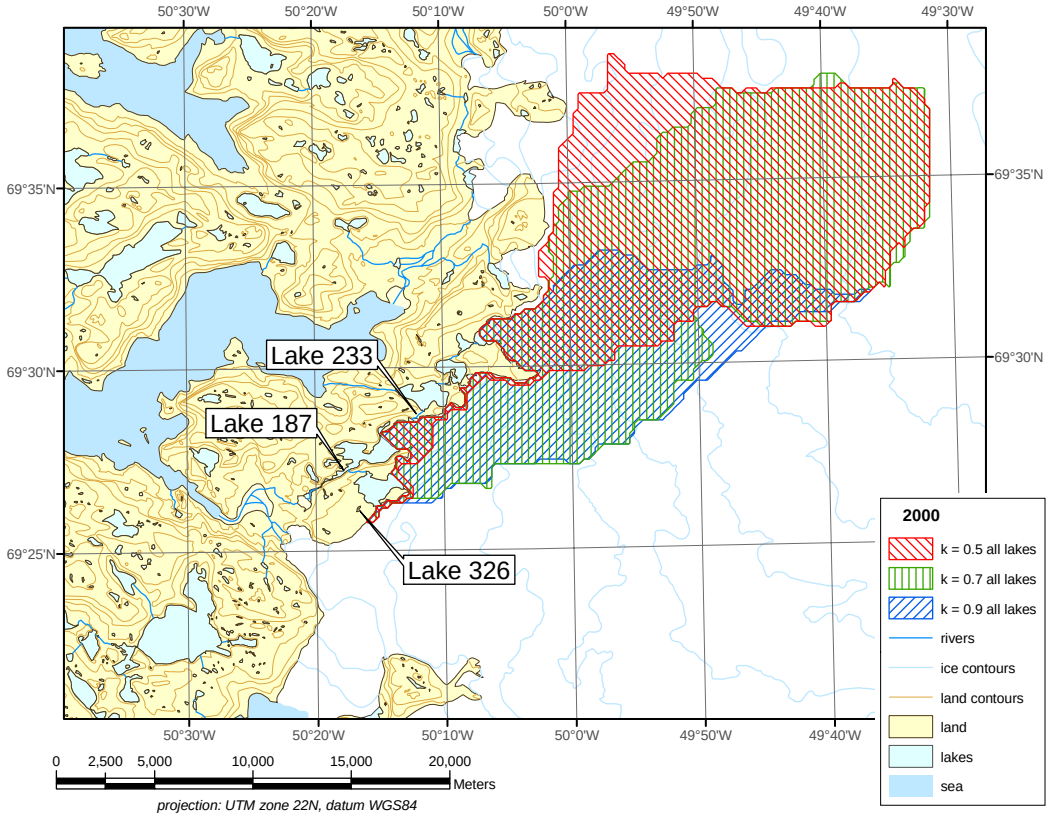

Figure 21. *The Paakitsoq area of the margin in 2000 showing the drainage basins predicted for all lakes for three different values of the k-factor*

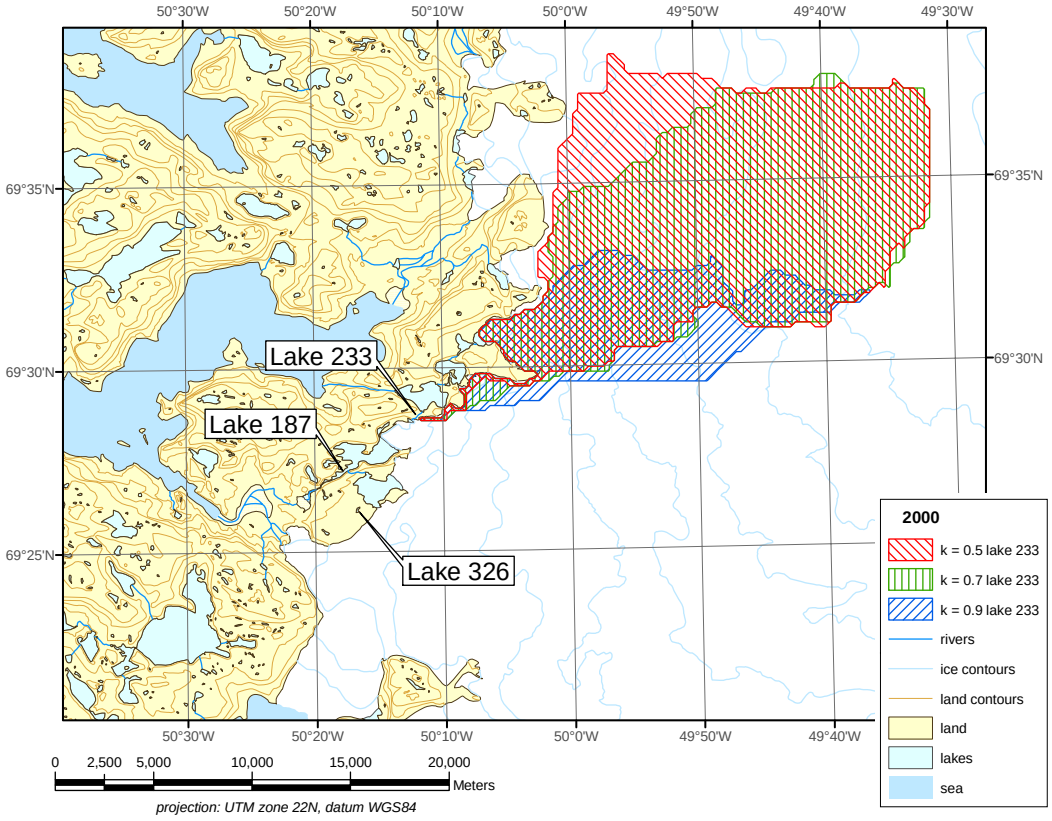

Figure 22. *The Paakitsoq area of the margin in 2000 showing the drainage basins predicted for lake 233 for three different values of the k-factor*

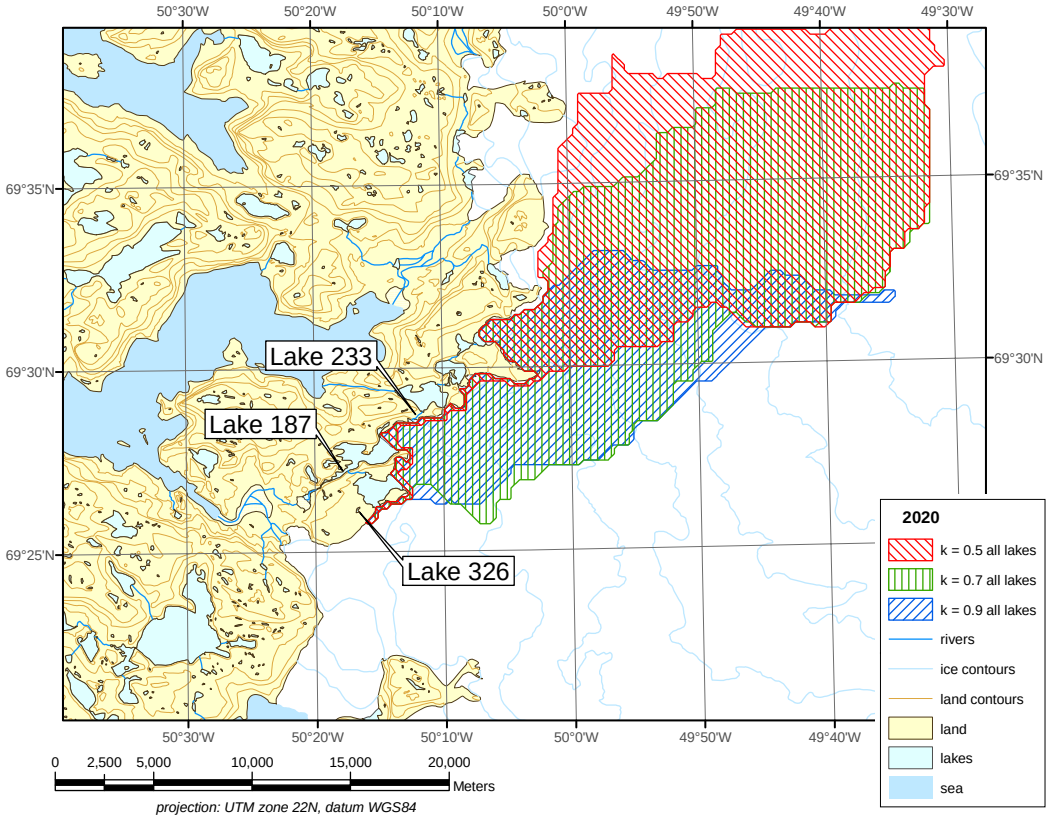

Figure 23. *The Paakitsoq area of the margin in 2020 showing the drainage basins predicted for all lakes for three different values of the k-factor*

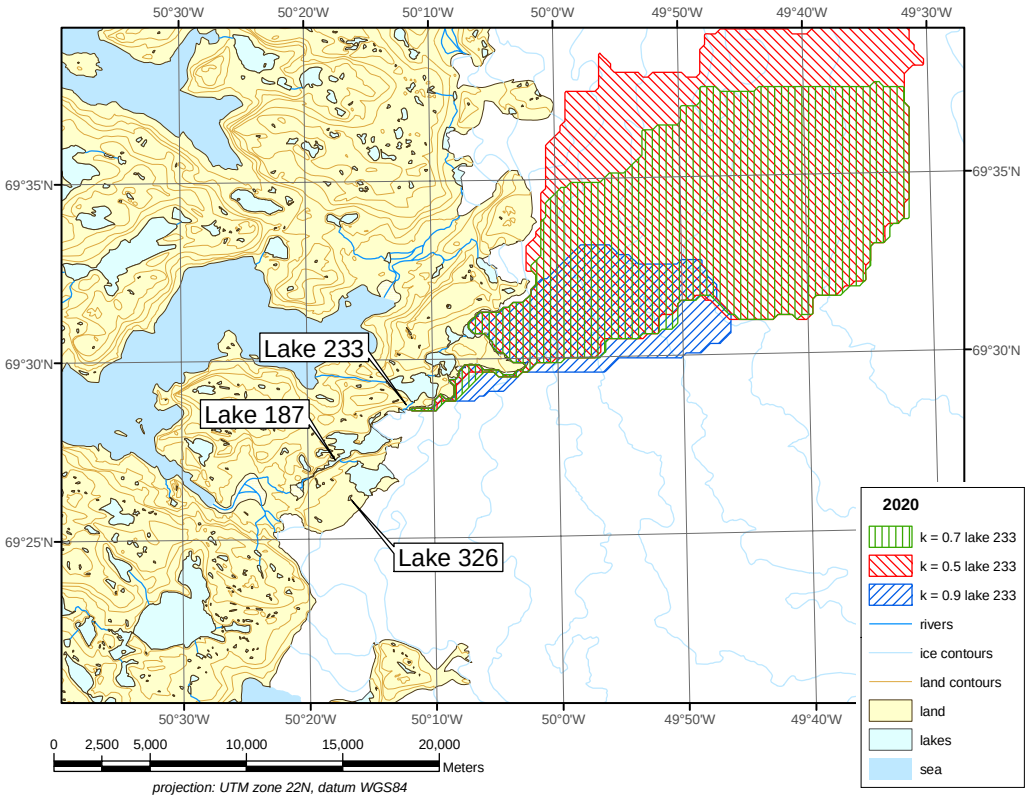

Figure 24. *The Paakitsoq area of the margin in 2020 showing the drainage basins predicted for lake 233 for three different values of the k-factor*

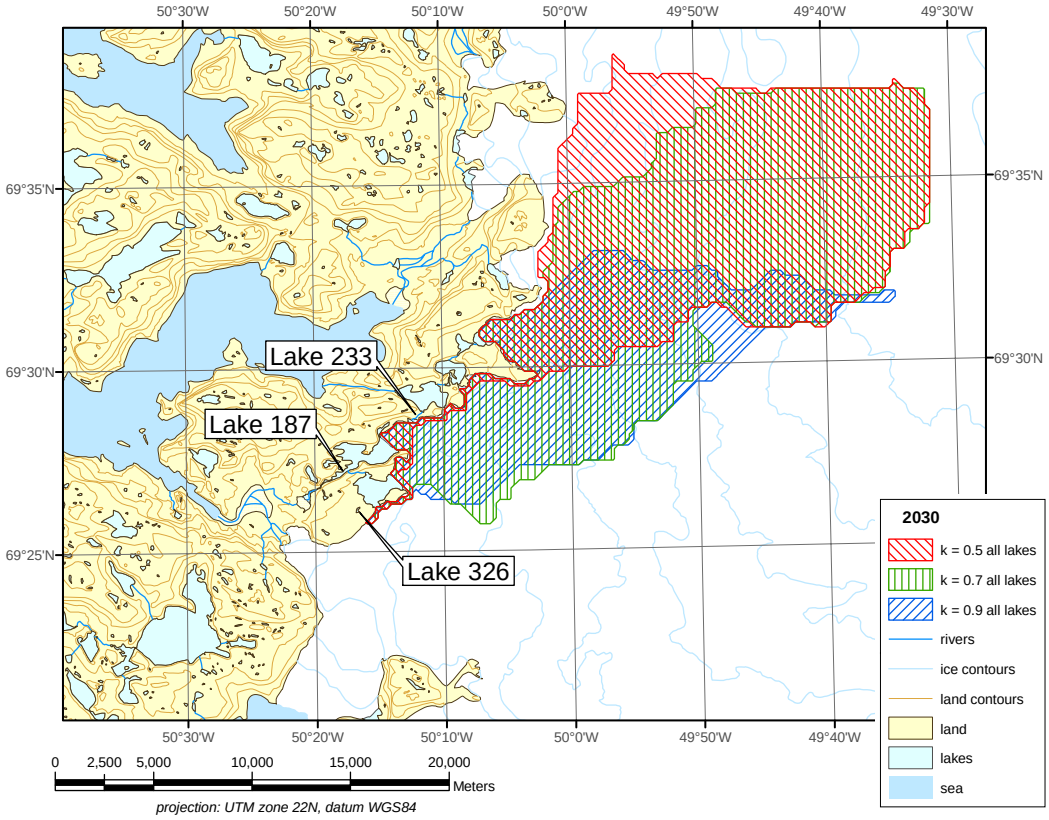

Figure 25. *The Paakitsoq area of the margin in 2030 showing the drainage basins predicted for all lakes for three different values of the k-factor*

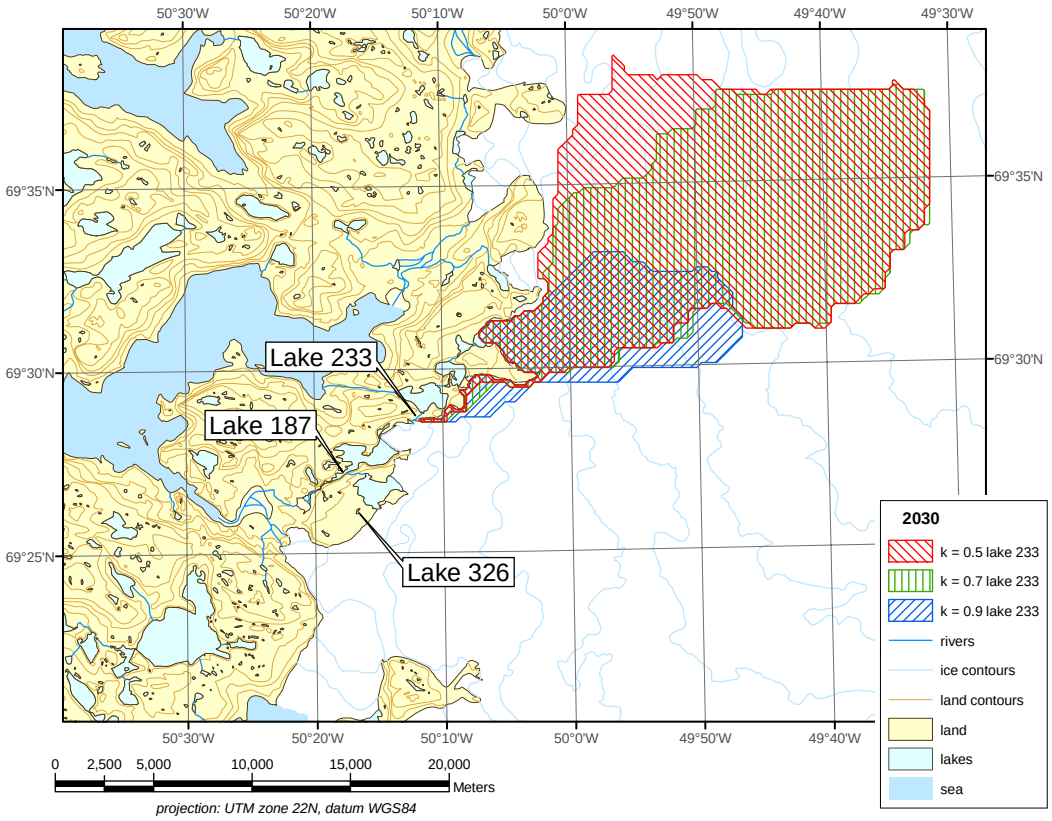

Figure 26. *The Paakitsoq area of the margin in 2030 showing the drainage basins predicted for lake 233 for three different values of the k-factor*

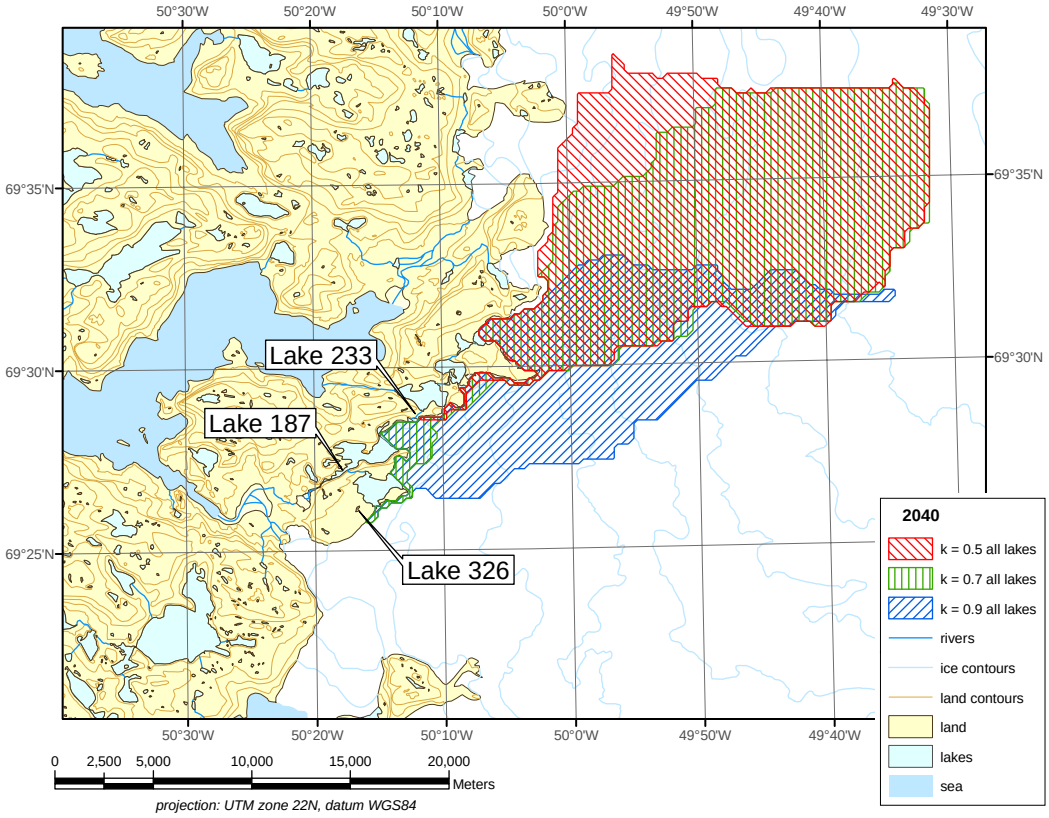

Figure 27. *The Paakitsoq area of the margin in 2040 showing the drainage basins predicted for all lakes for three different values of the k-factor*

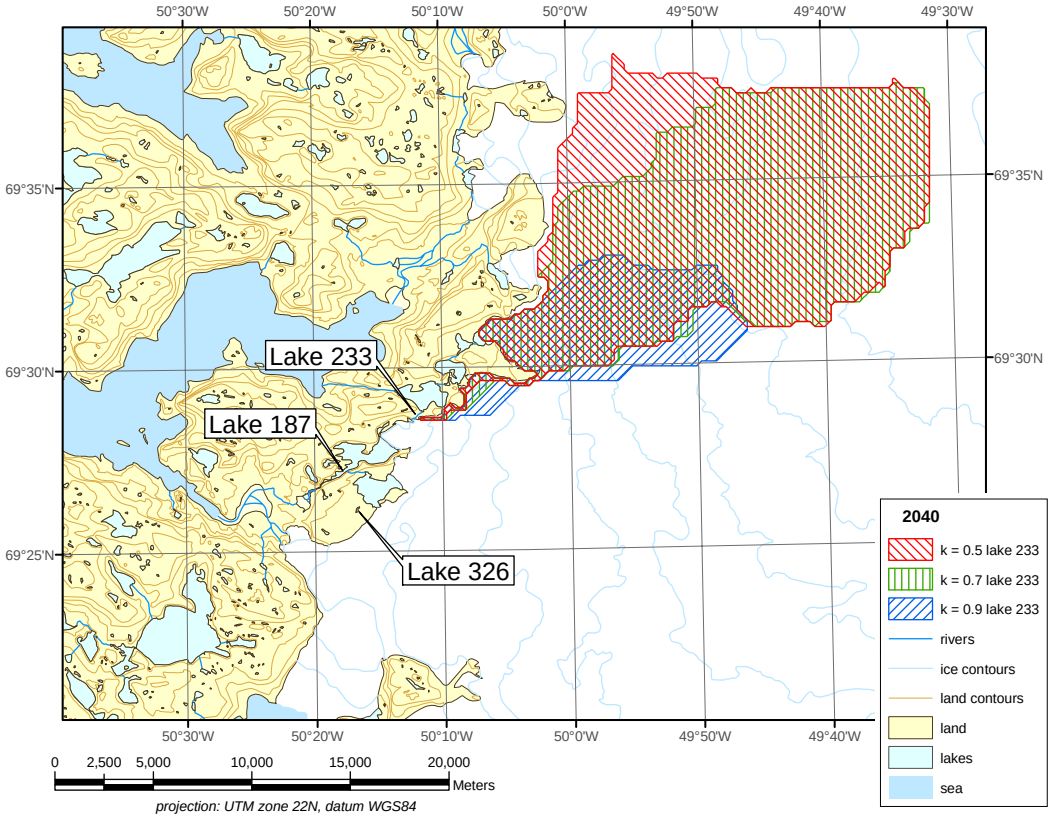

Figure 28. *The Paakitsoq area of the margin in 2040 showing the drainage basins predicted for lake 233 for three different values of the k-factor.*

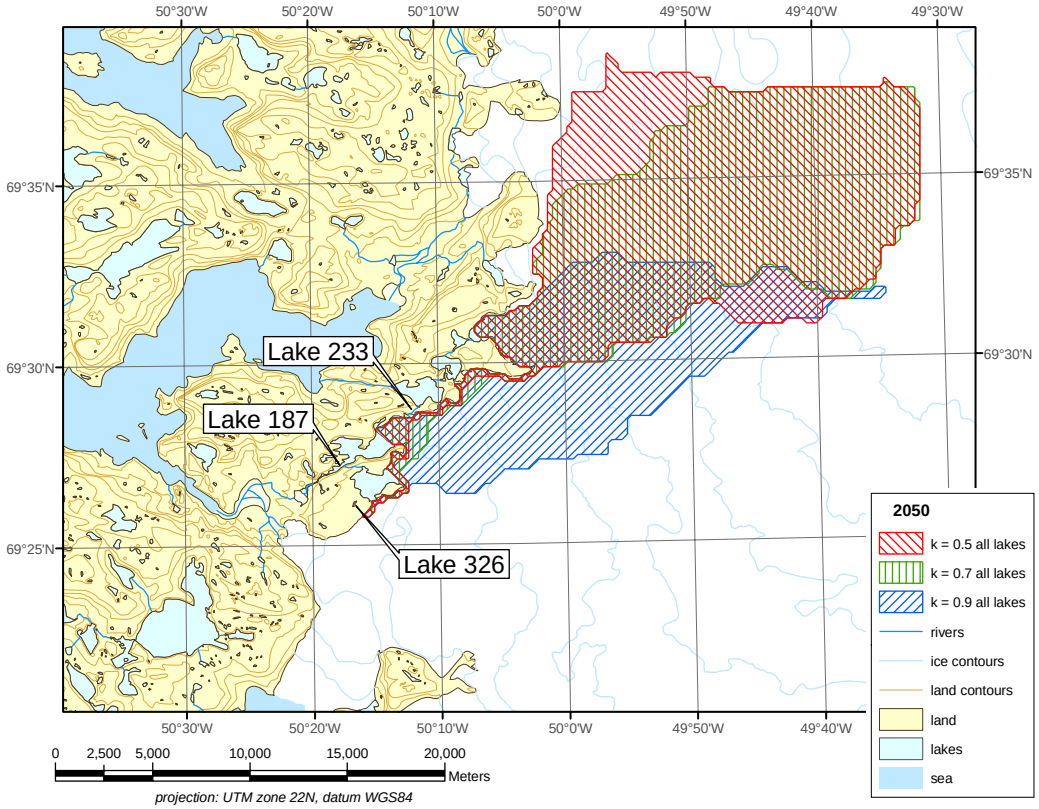

Figure 29. *The Paakitsoq area of the margin in 2050 showing the drainage basins predicted for all lakes for three different values of the k-factor.*

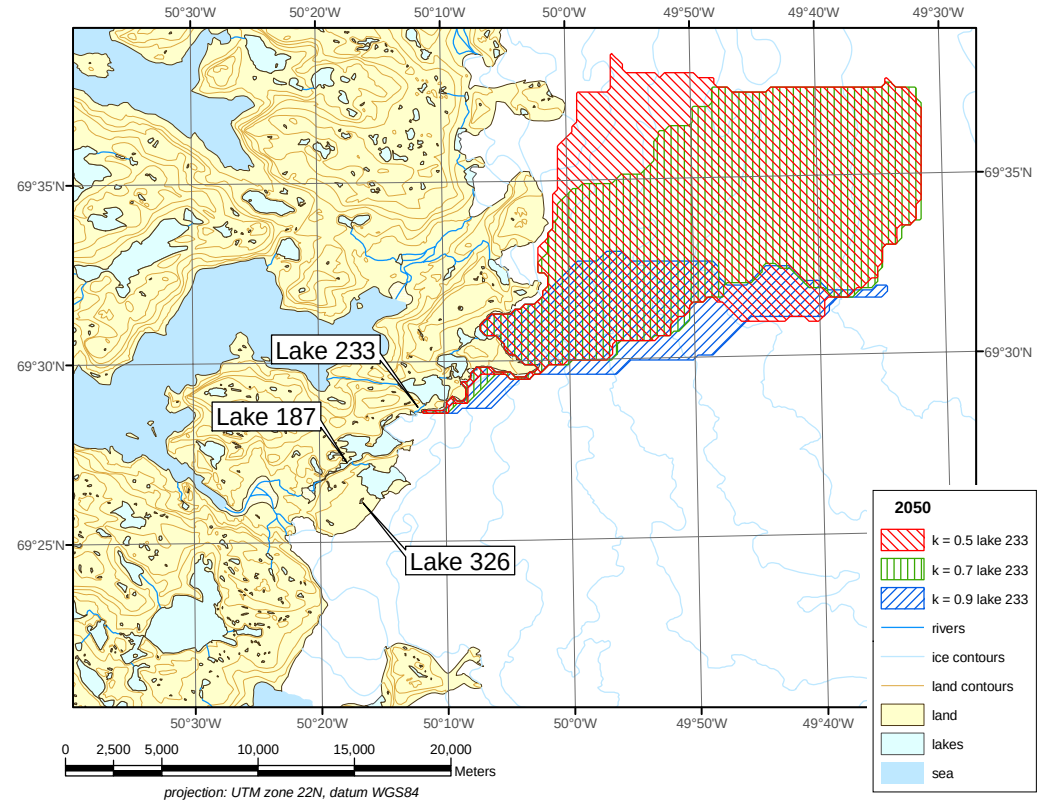

Figure 30. *The Paakitsoq area of the margin in 2050 showing the drainage basins predicted for lake 233 for three different values of the k-factor.*

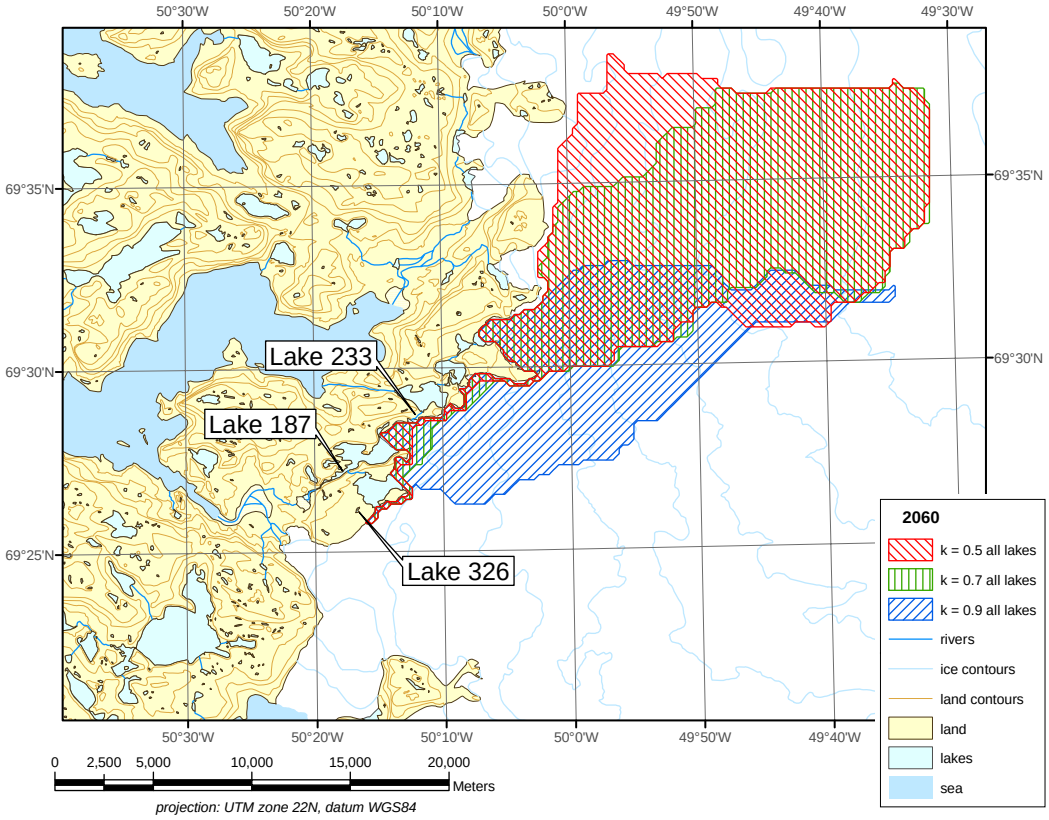

Figure 31. *The Paakitsoq area of the margin in 2060 showing the drainage basins predicted for all lakes for three different values of the k-factor.*

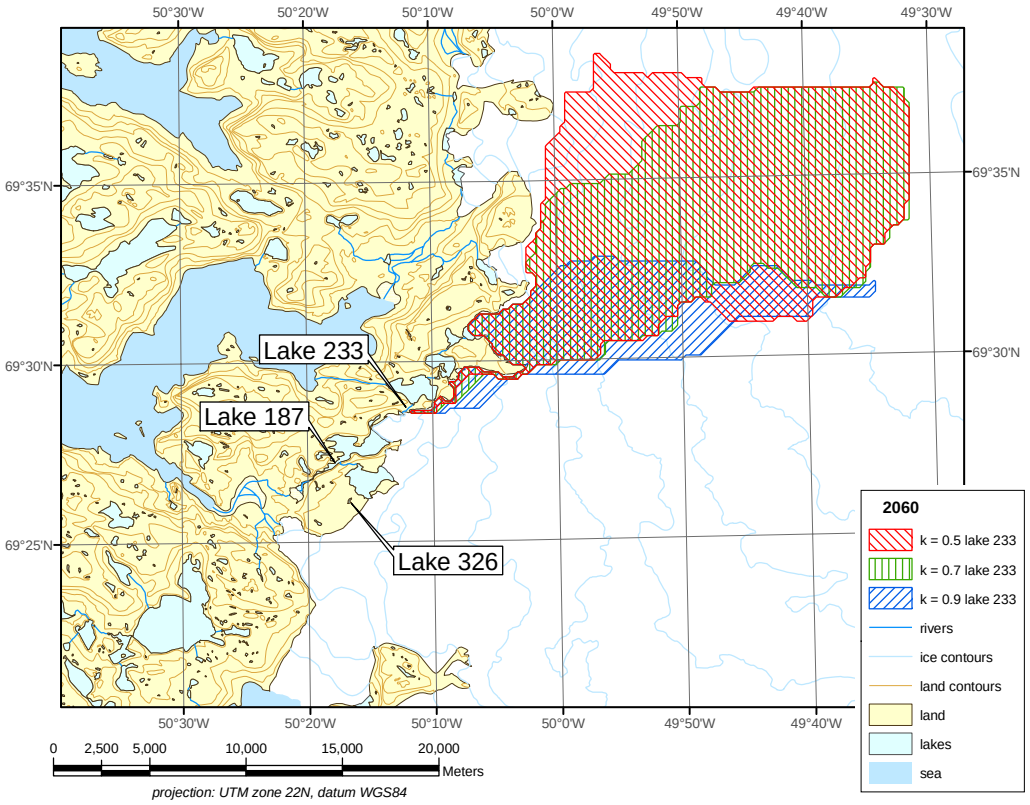

Figure 32. *The Paakitsoq area of the margin in 2060 showing the drainage basins predicted for lake 233 for three different values of the k-factor.*

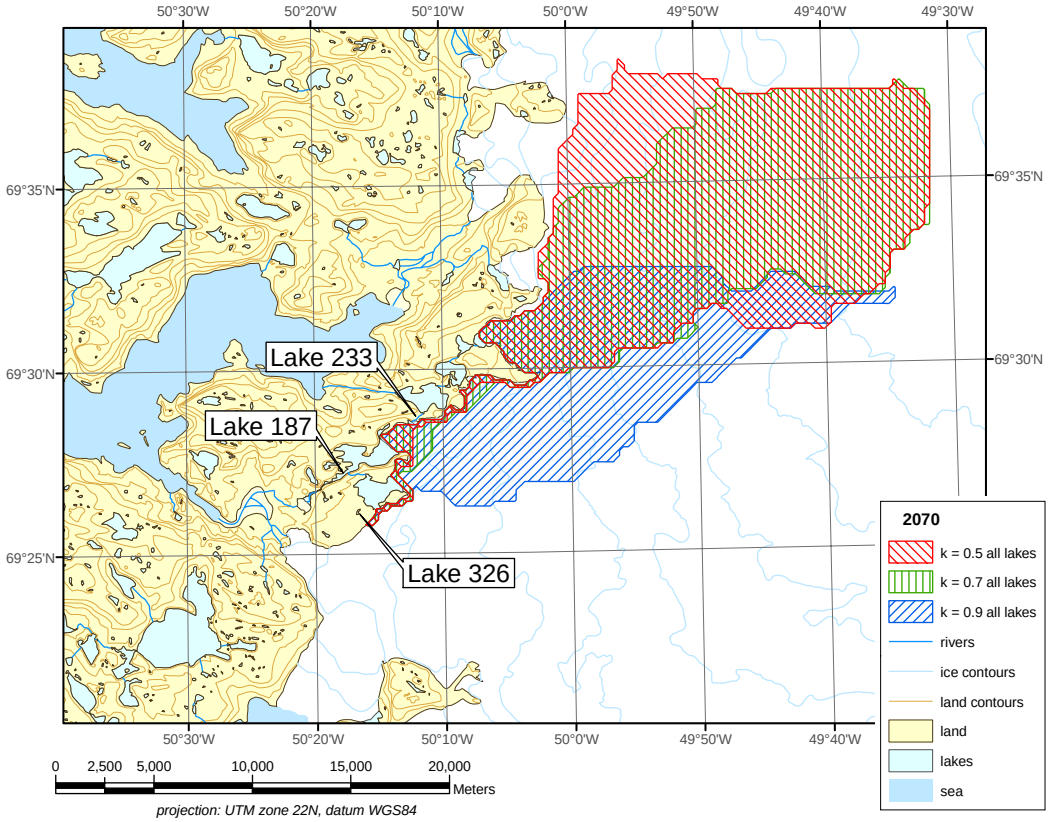

Figure 33. *The Paakitsoq area of the margin in 2070 showing the drainage basins predicted for all lakes for three different values of the k-factor.*

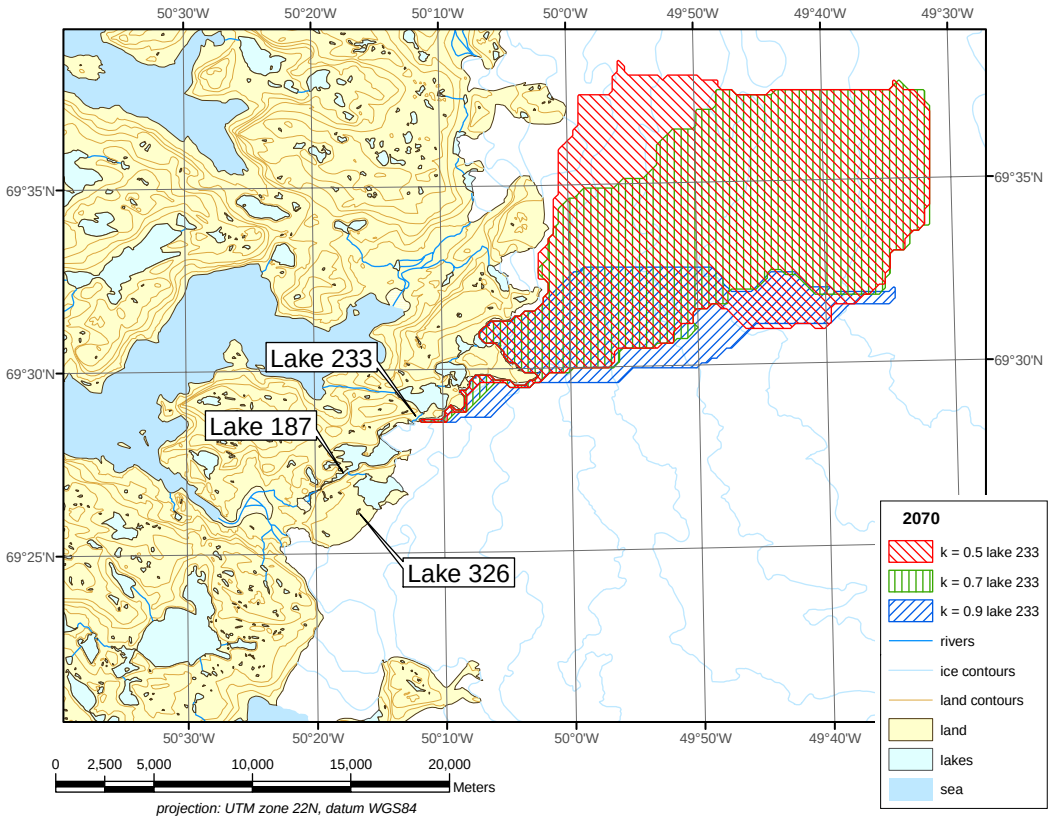

Figure 34. *The Paakitsoq area of the margin in 2070 showing the drainage basins predicted for lake 233 for three different values of the k-factor.*

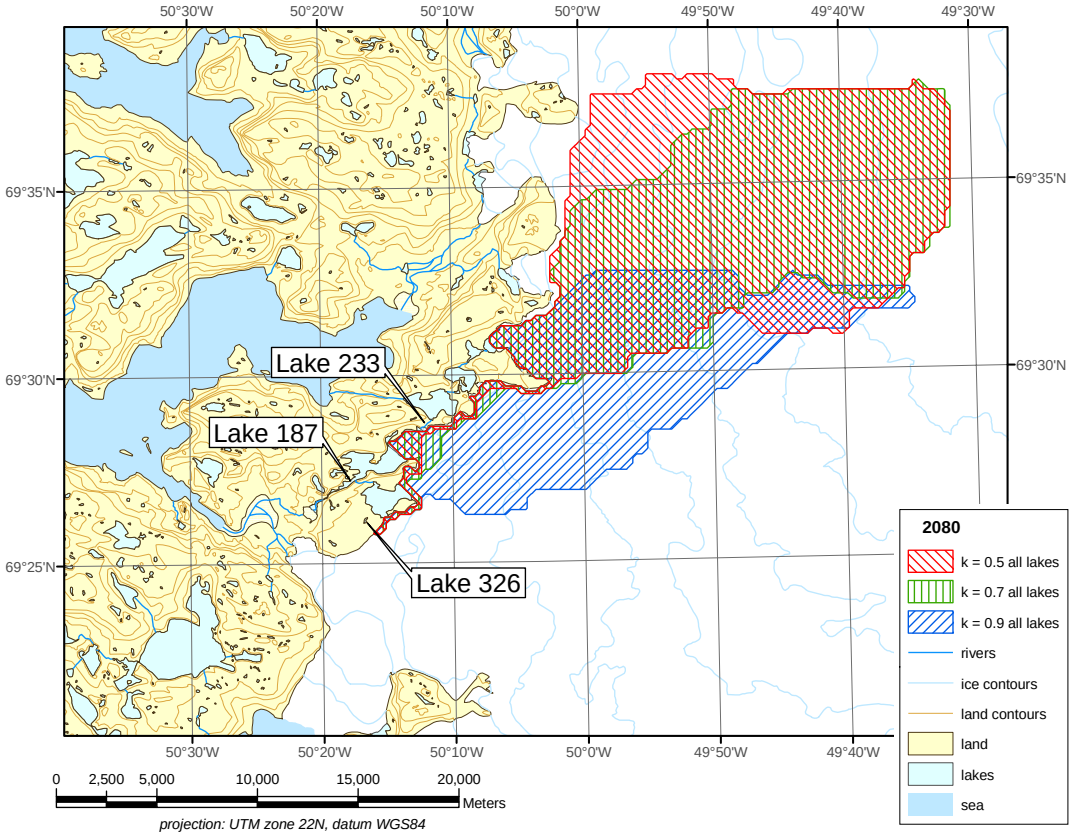

Figure 35. *The Paakitsoq area of the margin in 2080 showing the drainage basins predicted for all lakes for three different values of the k-factor.*

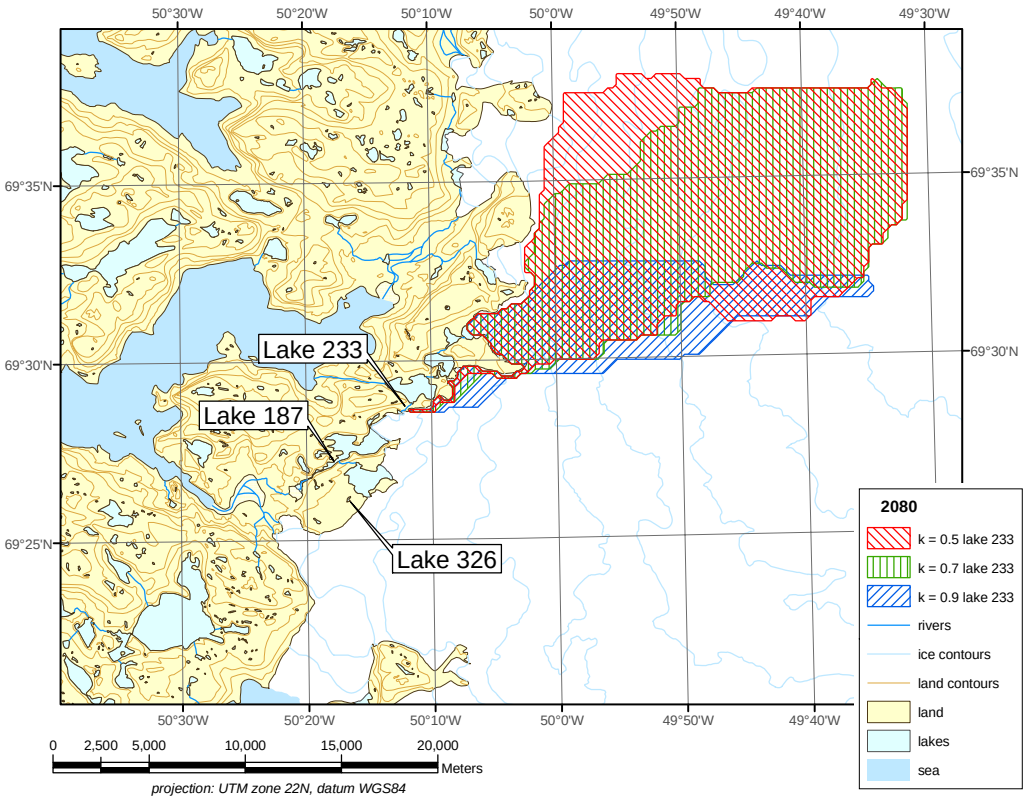

Figure 36. *The Paakitsoq area of the margin in 2080 showing the drainage basins predicted for lake 233 for three different values of the k-factor.*

The most important result from the basin configuration analysis is that the drainage basins are predicted to change relatively little up to 2080. Following the delineation of the drainage basins, the melt model was applied to each catchment in order to calculate the discharge from each for a range of values of k.

7. Conclusion

A combined global/regional climate model (HIRHAM4) scenario covering 1950–2080 was downscaled to catchment scale and corrected using observational data. Subsequently, the corrected HIRHAM4 output was used as input to a temperature-index mass-balance model in turn forcing an ice-dynamic model in order to predict the future ice sheet geometry. Together with a detailed map of subglacial topography produced from ice-penetrating radar data, these ice sheet geometries were used to predict the size of the ice-sheet part of the hydrological basin Pakitsup Akuliarusersua for a range of 11 different levels of basal water pressure every 10 years from present day to 2080.

Thus, the present analysis takes into account global and regional climate change, ice-dynamical response and changes in the internal drainage system of the ice sheet. However, care should be taken in the use of the predictions presented for a number of reasons:

- Our analysis shows that the HIRHAM4 output needs substantial adjustment to reproduce observations on catchment scale
- Ice-dynamic models do not yet capture all the important processes of the ice sheet, in particular its dynamic response to an increase in the surface meltwater input to its internal drainage system
- Our knowledge of the internal drainage of the Greenland ice sheet is insufficient to model the likely evolution and distribution of the basal water pressure, which may cause changes in the basin delineation and thus the discharge

The ice-sheet margin is predicted to continue its present thinning trend, causing a thinning of approx. 80 metres over the next 70 years as shown in Figures 18-20. This corresponds roughly to the current rate of ice-sheet thinning in the region amounting to approx. 1 metre per year on average over the last 40 years. The predicted retreat rates seem realistic from a glaciological point of view and cause only minor changes in the basin delineation for high (realistic) basal water pressures. Figure 37 shows the modelled evolution of the basin corresponding to a basal water pressure of 90% of the ice overburden pressure (k = 0.90) from 2000 to 2080. Measurements in boreholes drilled through the ice near the ice-sheet margin within the basin late in the melt season, points at basal water pressures ranging between 79% and 105% of the ice overburden pressure.

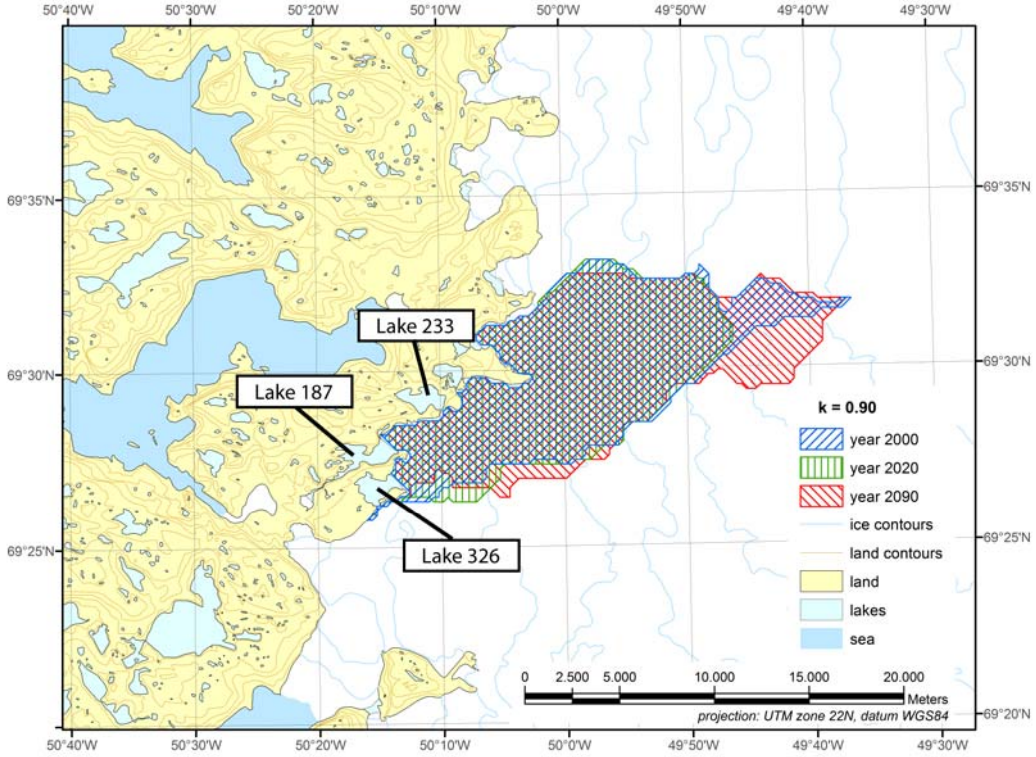

Figure 38. *The modelled evolution of the drainage basin configuration for a constant basal water pressure of 90% of the ice overburden pressure (k=0.90). The selected years show the maximum variation of the basin delineation.*

The basal water pressure varies diurnally, annually and may possibly shift over longer time scales if melt rates increase. The time of year (late melt season) and the proximity of the ice margin implies that this range should be taken as a minimum value. Choosing 90% (or k = 0.90) as a reference value to calculate discharge therefore makes sense. Further away from the ice margin, where the ice is thicker, the basal water pressure is likely to be higher rather than lower than 90% of the ice overburden pressure. This is important when examining basin delineation changes. However, in order to assess the extreme cases of lower basal water pressures, values of k ranging from k = 0.50 to k = 1.00 in increments of 0.05 were examined for the entire model period 1950 to 2080. Figure 39 shows the maximum variability of the basin configuration with basal water pressure for the year 2000 (present-day ice sheet geometry).

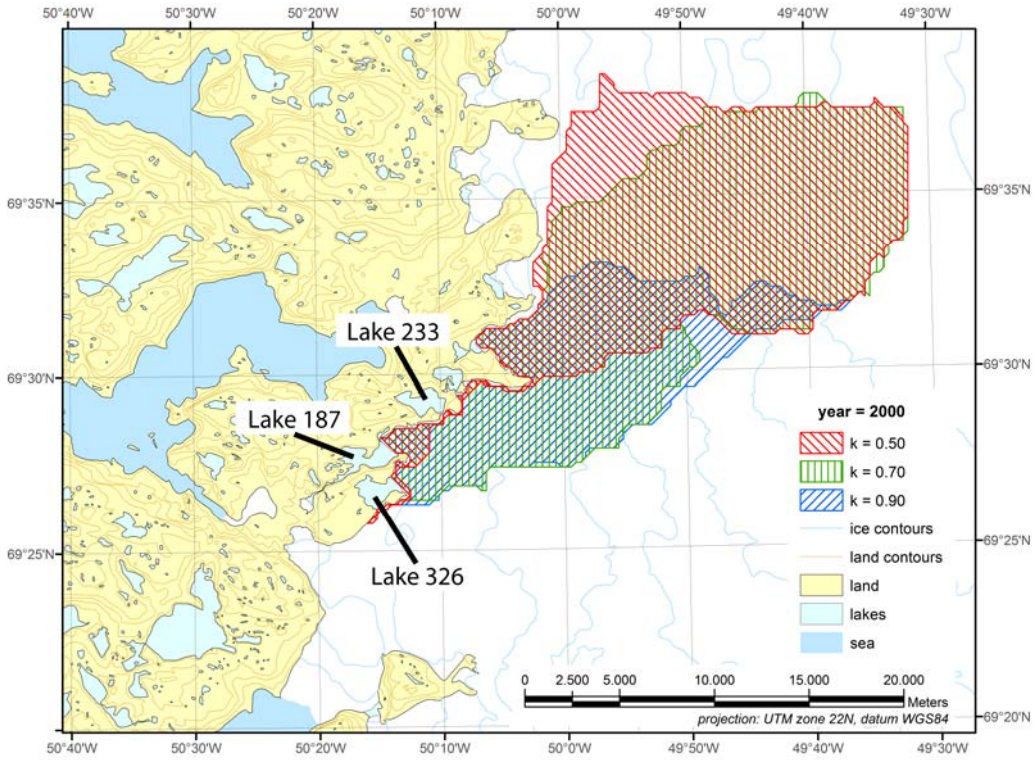

Figure 39. *Basin delineations for different values of basal water pressure, ranging from 50% to 90% of the ice overburden pressure. Measurements indicate a present minimum value between 79% and 105%. The values of k were chosen to show the different extremes in basin configuration.*

The HIRHAM4 model does not capture the development in the local climate of the catchment on a year-by-year basis, but is designed to show the large-scale trends. Our melt model input from HIRHAM4 was adjusted after comparing to observations in the catchment. After melt model calibration (carried out using k=0.90) we obtain 109% (435.5 hm^3) of the observed mean (398.3 hm^3) over 1985–2007, after removing known lake outburst floods in 1989 and 1993 and noting that there was inadequate or no data from 1984, 1988, 1991, 1992 and 1994. We believe that the absolute values of the predicted discharge shown in Figure 40 should be regarded as a minimum discharge estimate for the future, due to the choice of a conservative climate scenario. Our discharge prediction for 2014–2039 has a mean value of 414 hm^3 which corresponds to almost no change compared to a modelled mean of 418 hm^3 over 2000–2006. The main conclusion to draw from the inclusion of the HIRHAM4 model output (based on the IPCC SRES B2 scenario) in the discharge prediction is that the current average discharge of 443 hm^3 is likely to remain relatively constant until 2035, at which point a steady increase in the discharge sets in continuing to 2080. The last decade 2071–2080 is predicted to have a mean modelled discharge of 696 hm^3. This increase is driven by climate warming rather than changes in basin delineation.

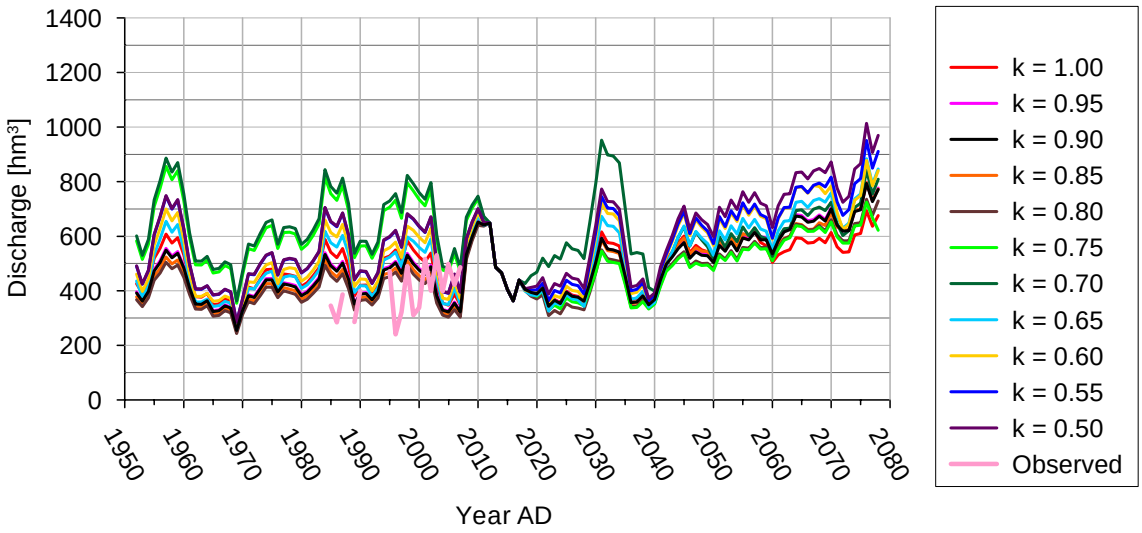

Figure 40. *Predicted discharge, shown as 5-year running averages, for various levels of basal water pressure, ranging from k=0.50 (low water pressure) to k=1.00 (ice nearly floating). The retreat of the ice sheet margin is causing drops in discharge for k=0.70 to k=0.80, due to rearrangement of the ice-sheet hydrological basin. The value of k is expected to have a minimum value between 0.79 and 1.05 from previous borehole measurements in the area.*

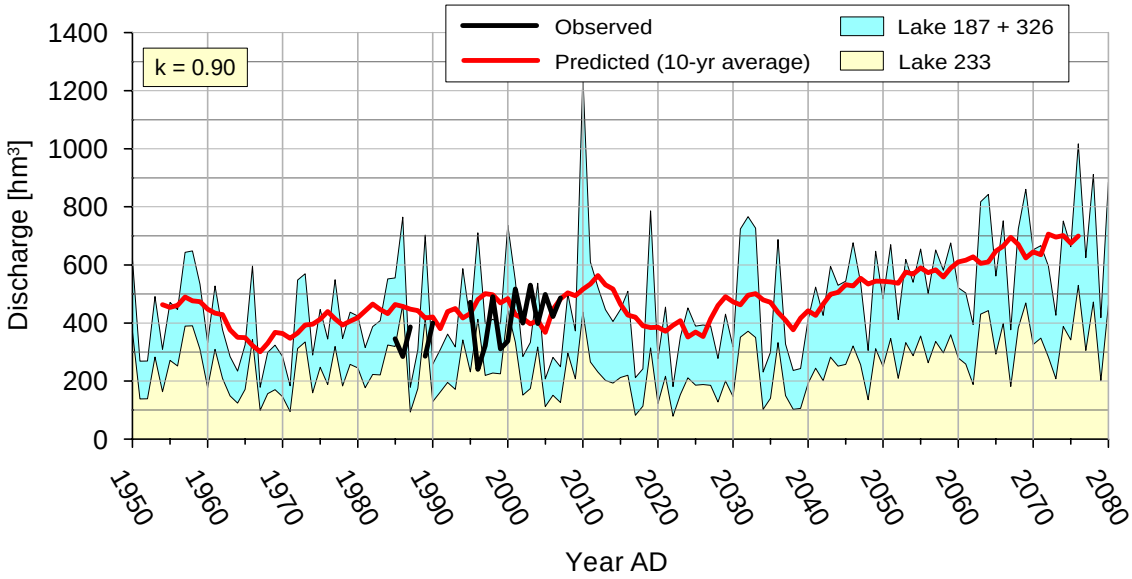

Figure 41. *Predicted and observed discharge from the Pakitsup Akuliarusersua basin, with division between Lakes 187 + 326 and Lake 233. The prediction shown is based on a high basal water pressure, close to what has previously been measured in boreholes in this part of the ice margin (k=0.90). This prediction of the discharge is considered the most likely***.**

The main conclusions can be summarized as follows

- The configuration of the ice-sheet hydrological basin is likely to remain constant
- As a minimum, the basin discharge is likely to remain constant until 2035, followed by a steady increase towards 2080
- The ice-sheet margin is likely to keep thinning at the current rate of approx. 1 m/yr

The first conclusion implies that the hydrological basin supplying the water to the lakes adjoining the ice sheet margin is not likely to change. This reduces the main risk of relying on

ice sheet catchments for hydropower production. The second conclusion implies that climate change will, as a minimum, have a small positive influence on the discharge increasing after 2035. The third conclusion reduces the risk of a readvance of the ice sheet margin that could potentially change the way the lakes connect in the off-ice-sheet part of the basin.

8. References

Ahlstrøm, A.P. (2007). Previous glaciological activities related to hydropower at Paakitsoq, Ilulissat, West Greenland. Geological Survey of Denmark and Greenland Report 2007/25.

Ahlstrøm, A.P., C.E. Bøggild, O.B. Olesen, D. Petersen, J.J. Mohr. (2007). Mass balance of the Amitsulôq ice cap, West Greenland, IAHS Publ. 318, p.107–115.

Ahlstrøm, A. P., Mohr, J.J., Reeh, N., Christensen, E.L., Hooke, R.LeB. (2005). Controls on the water pressure in subglacial channels near the margin of the Greenland Ice Sheet. Journal of Glaciology 174: 443-450.

Ahlstrøm, A. P. (2003). Ice sheet ablation assessed by observation, remote sensing and modelling. Geological Survey of Denmark and Greenland PhD Thesis.

Ahlstrøm, A. P., Bøggild, C.E., Mohr, J.J., Reeh, N., Christensen, E.L., Olesen, O.B., Keller, K. (2002). Mapping of a hydrological ice sheet drainage basin on the West Greenland ice-sheet margin from ERS-1/-2 SAR interferometry, ice radar measurement and modelling. Annals of Glaciology 34(309-314).

Bjornsson, H. (1982). "Drainage basins on Vatnajokull Mapped by radio echo soundings." Nordic Hydrology 13(4): 213-232.

Bogorodsky, V. V., C. R. Bentley, and P. E. Gudmandsen. (1985). Radioglaciology. D. Reidel, Dordrecht.

Das, S.B.,Joughin, I., Behn, M.D., Howat, I.M., King, M.A., Lizarralde, D., Bhatia, M.P. (2008). Fracture Propagation to the Base of the Greenland Ice Sheet During Supraglacial Lake Drainage. Science: 1153360.

Ekholm, S. (1996). "A full coverage, high-resolution, topographic model of Greenland computed from a variety of digital elevation data,." Journal of Geophysical Research-Solid Earth 101(B10): 21961-21972.

Kitanidis, P. K. (1997). Introduction to Geostatistics. Cambridge, Cambridge University Press.

Hagen, J.O., Etzelmuller, B., Nutall, A.M.(2000). Runoff and drainage pattern derived from digital elevation models, Finsterwalderbreen, Svalbard. Annals of Glaciology 31: 147-152.

Hempel, L., Thyssen, F., Gundestrup, N., Clausen, H.B., Miller, H. (2000). A comparison of radio-echo sounding data and electrical conductivity of the GRIP ice core. Journal of Glaciology, 46, 154, 369-374.

Hock, R. (2003). Temperature index melt modelling in mountain areas. Journal of Hydrology 282 (1-4): 104-115.

Joughin, I., Das, S.B., King, M.A., Smith, B.E., Howat, I.M., Moon, T. (2008). Seasonal Speedup Along the Western Flank of the Greenland Ice Sheet. Science, 10.1126/science.1153288

Nakicenovic, N. and Swart, R. (eds). 2000: IPCC Special Report on Emission Scenarios, Cambridge University Press, 612 pp.

Reeh, N. (1991). Parameterization of melt rate and surface temperature on the Greenland ice sheet. Polarforschung, 59 (3), 113-128.

Reeh, N. (1988). A flow-line model for calculating the surface profile and the velocity, strain-rate, and stress fields in an ice sheet, Journal of Glaciology, Vol. 34 (116), p.46–54.

Reeh, N., Ahlstrøm, A. (2005). Nordic Project on Climate and Energy, Subproject Hydropower, Snow and Ice. Danish National Space Centre, Technical University of Denmark.

Shreve, R. L. (1972). Movement of water in glaciers. Journal of Glaciology 11(62): 205-214.

Steffen, K., Box, J. (2001). Surface Climatology of the Greenland ice sheet: Greenland Climate Network 1995-1999. Journal of Geophysical Research 106(D24): 33951-33964.

Thomsen, H. H. Thorning, L., Braithwaite, R.J. (1988). Glacier-hydrological conditions on the Inland Ice north-east of Jakobshavn/Ilulissat, West Greenland. Geological Survey of Denmark and Greenland Report 138.

Zwally, H.J., Abdalati, W., Herring, T., Larson, K., Saba, J., Steffen,K.(2002). Surface Melt-Induced Acceleration of Greenland Ice-Sheet Flow Science 297 (5579) [DOI: 10.1126/science.1072708]

Appendices

The aim of these appendices is to give a step by step guide to the individual stages in the process of evaluating the hydropower potential of this area, in order to facilitate similar studies.

Appendix A – Radar Processing

1. First catch your data: Collect radar data, process and convert to ramac format.
- Import into ReflexW's 2D data analysis module
- Set X start and X end values to coincide with trace numbers.

2. Processing: Within ReflexW
- ***Dewow*** with a value in the case of around 2000 ns, this removes noise by averaging the value over a number of pixels (in this case ~25)
- ***Gain*** processing enhances the energy decay, a value of around 2 to 4 worked best for this dataset

3. Digitising and picking: The continuous pick method was found to be best for digitising the surface and basal lines. This enables a continuous line of picks to be selected by holding down the mouse button. Alternatively select a single pick with a single click. Use the interpolate button in difficult areas to interpolate a line between two clear pick points.

4. Defining layers: Once a single layer has been digitised, export the file in ASCII format (.pck) with a trace number and travel time in separate columns. The trace number is used to match up the digitised layers with the geographical coordinates

5. Calculating elevation:
Within excel (or similar) match the data for 2 way travel times with geographical positioning information based on the recorded trace numbers.
Apply the following equation to each line of data:

$$H_s = H_p - 0.5 \cdot t_S v_{air}$$

$$H_i = 0.5 \cdot (t_B - t_S) \cdot v_{ice}$$

$$H_b = H_s - H_i$$

H_s = surface elevation, H_p = measured elevation of the plane, t_s= 2 way travel time to the surface, v_{air} = velocity of light through air, H_i = ice thickness, t_b= 2 way travel time to the bed v_{ice} = velocity of light through ice, H_b = bed elevation

6. DEM creation: Export coordinates and elevations to Surfer. Create DEMs of bed and surface using kriging or other interpolation method.

Appendix B - Climate Data Processing

1.Input grids: Three grids are needed for the model as inputs, these must be prepared carefully and with the same dimensions and grid spacing in the ASCII format. These are:
- Surface elevation
- Modelled precipitation
- Modelled temperature

⇩

2.Surface elevation: Use the surface DEM grid created from the lidar data merged with the larger scale DEMs. For this project the format was:
400 rows x 598 columns
X minimum 501557
X maximum 1098542
Y minimum 7650354
Y maximum 8049663

⇩

3a.Modelled temperature grids: based on DMI modelled daily values, average the temperatures to monthly means. Use the DMI temperature data for 2m above the surface and the lapse rates given by Steffen and Box (2001). Procedure:
i) Find the difference in elevation between the project DEM and the model DEM grids, to create a difference grid
ii) Multiply the difference grid by monthly lapse rates, to give monthly temperature difference grids
iii) Krig the DMI 25 km temperature grids to the 1km grid size and format
iv) Add the temperature difference grids to the 1km DMI 2m surface temperature grids for each month.

⇩

3b.Additional temperature correction: The lapse rate is very localised so a further correction is required to give reasonable values before the model is run:
i) Calculate daily mean temperatures from hourly measurements at local weather stations
ii) Find closest value from lapse corrected temperature grids and in excel compare with measurements.
iii) Use these corrections in the following melt model

⇩

4.Modelled precipitation grids: based on DMI modelled annual precipitation. Note that this is not scaled with a lapse rate as there is insufficient data to determine one.
i) Krig the DMI 25 km precipitation grid to the 1km grid size and area for each year.

Appendix C – Melt Modelling

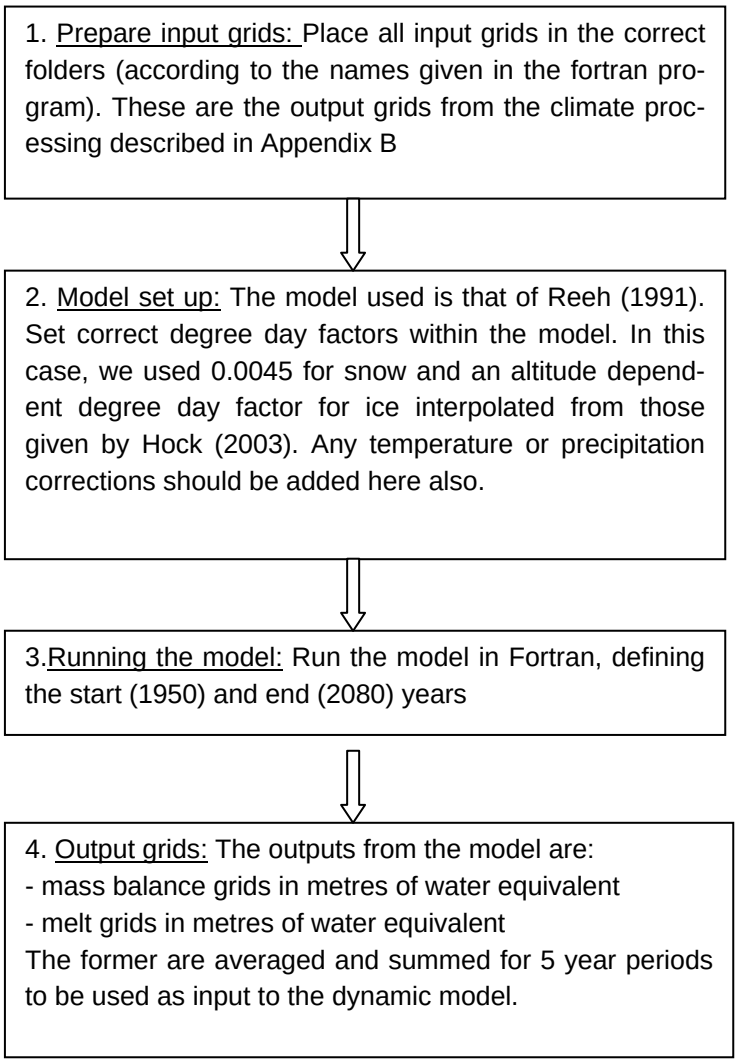

Appendix D – Dynamic Modelling

1. Prepare input grids: Create initial surface grid and use this and the basal grid to calculate ice thickness, terrain aspect and plan curvature grids using the grid math and grid calculus functions in Surfer. Save the average mass balance grid to the right filename.
Using the digitise command in surfer, select one point at the margin for which the flowline to the centre is required. Save this point as digit.dat.

⇩

2. Running the model: Check the flow.ini and dynamic.ini initialisation files and run the programs in the following order:
Flow.FOR - Calculates flow line based on topography
Dynamic_1000.BAS – Extracts data from input grids along profile
Dynamic.FOR – Calculates velocity, strain, stress along flow
Uwscalcd.FOR – Calculates surface elevation and ice thickness
Flowline1.BAS – plots output values

⇩

3. Export values: Import output from the following files to the flowlines.xls spreadsheet, then repeat model runs for successive flow lines, (if model being run for more than one profile):
Flow.BLN
Dprofcomp.DAT

⇩

4. Iteration: Add static mass balance change to elevation grid (static change = cumul. mass bal for Time2 – cumul. mass bal for Time1) and repeat steps 1-3 for following 5 year period.

⇩

5. Determine elevation changes: In flowlines.XLS calculate the difference between the predicted elevation profiles between the two periods, import this into grapher and determine polynomial best fit using the fit function.

⇩

6. Generalise elevation change: Export surface elevation grid as xyz.DAT file and within the worksheet apply the calculated polynomial as a transformation to the elevations. Krig, grid and save file as the new surface elevation.

Notes for Paakitsoq project:

a) Initial surface elevation was defined from lidar data and combined with surface elevation model.

b) Ensure all mass balance and elevation grids are the same size and have the same array structure or problems will occur!

c) The dynamic and surfer programs assume different things about the curvature grid, therefore it needs to be inverted once it has been created

Appendix E – Melt Discharge and Basin Delineation